II

Advanced Tracking and Association Methods

8 Target Tracking Using Probabilistic Data Association-Based Techniques with Applications to Sonar, Radar, and EO Sensors *T. Kirubarajan and Yaakov Bar-Shalom*
Introduction • Probabilistic Data Association • Low Observable TMA Using the ML-PDA Approach with Features • The IMMPDAF for Tracking Maneuvering Targets • A Flexible-Window ML-PDA Estimator for Tracking Low Observable (LO) Targets • Summary

9 An Introduction to the Combinatorics of Optimal and Approximate Data Association *Jeffrey K. Uhlmann*
Introduction • Background • Most Probable Assignments • Optimal Approach • Computational Considerations • Efficient Computation of the JAM • Crude Permanent Approximations • Approximations Based on Permanent Inequalities • Comparisons of Different Approaches • Large-Scale Data Associations • Generalizations • Conclusions • Acknowledgments • Appendix 9.A Algorithm for Data Association Experiment

10 A Bayesian Approach to Multiple-Target Tracking *Lawrence D. Stone*
Introduction • Bayesian Formulation of the Single-Target Tracking Problem • Multiple-Target Tracking without Contacts or Association (Unified Tracking) • Multiple-Hypothesis Tracking (MHT) • Relationship of Unified Tracking to MHT and Other Tracking Approaches • Likelihood Ratio Detection and Tracking

11 Data Association Using Multiple Frame Assignments *Aubrey B. Poore, Suihua Lu, and Brian J. Suchomel*
Introduction • Problem Background • Assignment Formulation of Some General Data Association Problems • Multiple Frame Track Initiation and Track Maintenance • Algorithms • Future Directions

12 General Decentralized Data Fusion with Covariance Intersection (CI) *Simon Julier and Jeffrey K. Uhlmann*
Introduction • Decentralized Data Fusion • Covariance Intersection • Using Covariance Intersection for Distributed Data Fusion • Extended Example • Incorporating Known Independent Information • Conclusions • Appendix 12.A The Consistency of CI • Appendix 12.B MATLAB Source Code (Conventional CI and Split CI)

13 Data Fusion in Nonlinear Systems *Simon Julier and Jeffrey K. Uhlmann*
Introduction • Estimation in Nonlinear Systems • The Unscented Transformation • Uses of the Transformation • The Unscented Filter • Case Study: Using the UF with Linearization Errors • Case Study: Using the UF with a High-Order Nonlinear System • Multilevel Sensor Fusion • Conclusions

14 Random Set Theory for Target Tracking and Identification *Ronald Mahler*
Introduction • Basic Statistics for Tracking and Identification • Multitarget Sensor Models • Multitarget Motion Models • The FISST Multisource-Multitarget Calculus • FISST Multisource-Multitarget Statistics • Optimal-Bayes Fusion, Tracking, ID • Robust-Bayes Fusion, Tracking, ID • Summary and Conclusions

8

Target Tracking Using Probabilistic Data Association-Based Techniques with Applications to Sonar, Radar, and EO Sensors

8.1 Introduction

8.2 Probabilistic Data Association
Assumptions • The PDAF Approach • Measurement Validation • The State Estimation • The State and Covariance Update • The Prediction Equations • The Probabilistic Data Association • The Parametric PDA • The Nonparametric PDA

8.3 Low Observable TMA Using the ML-PDA Approach with Features
Amplitude Information Feature • Target Models • Maximum Likelihood Estimator Combined with PDA — The ML-PDA • Cramér-Rao Lower Bound for the Estimate • Results

8.4 The IMMPDAF for Tracking Maneuvering Targets
Coordinate Selection • Track Formation • Track Maintenance • Track Termination • Simulation Results

8.5 A Flexible-Window ML-PDA Estimator for Tracking Low Observable (LO) Targets
The Scenario • Formulation of the ML-PDA Estimator • Adaptive ML-PDA • Results

8.6 Summary

References

T. Kirubarajan
University of Connecticut

Yaakov Bar-Shalom
University of Connecticut

8.1 Introduction

In tracking targets with less-than-unity probability of detection in the presence of false alarms (clutter), data association — deciding *which* of the received multiple measurements to use to update each track — is crucial. A number of algorithms have been developed to solve this problem.[1-4] Two simple solutions are the Strongest Neighbor Filter (SNF) and the Nearest Neighbor Filter (NNF). In the SNF, the signal

with the highest intensity among the validated measurements (in a gate) is used for track update and the others are discarded. In the NNF, the measurement closest to the predicted measurement is used. While these simple techniques work reasonably well with benign targets in sparse scenarios, they begin to fail as the false alarm rate increases or with low observable (low probability of target detection) maneuvering targets.[5,6] Instead of using only one measurement among the received ones and discarding the others, an alternative approach is to use all of the validated measurements with different weights (probabilities), known as Probabilistic Data Association (PDA).[3] The standard PDA and its numerous improved versions have been shown to be very effective in tracking a single target in clutter.[6,7]

Data association becomes more difficult with multiple targets where the tracks compete for measurements. Here, in addition to a track validating multiple measurements as in the single target case, a measurement itself can be validated by multiple tracks (i.e., contention occurs among tracks for measurements). Many algorithms exist to handle this contention. The Joint Probabilistic Data Association (JPDA) algorithm is used to track multiple targets by evaluating the measurement-to-track association probabilities and combining them to find the state estimate.[3] The Multiple-Hypothesis Tracking (MHT) is a more powerful (but much more complex) algorithm that handles the multitarget tracking problem by evaluating the likelihood that there is a target given a sequence of measurements.[4] In the tracking benchmark problem[8] designed to compare the performance of different algorithms for tracking highly maneuvering targets in the presence of electronic countermeasures, the PDA-based estimator, in conjunction with the Interacting Multiple Model (IMM) estimator, yielded one of the best solutions. Its performance was comparable to that of the MHT algorithm.[6,9]

This chapter presents an overview of the PDA technique and its application for different target-tracking scenarios. Section 8.2 summarizes the PDA technique. Section 8.3 describes the use of the PDA technique for tracking low observable targets with passive sonar measurements. This target motion analysis (TMA) is an application of the PDA technique, in conjunction with the maximum likelihood (ML) approach for target motion parameter estimation via a batch procedure. Section 8.4 presents the use of the PDA technique for tracking highly maneuvering targets and for radar resource management. It illustrates the application of the PDA technique for recursive state estimation using the IMMPDAF. Section 8.5 presents a state-of-the-art sliding-window (which can also expand and contract) parameter estimator using the PDA approach for tracking the state of a maneuvering target using measurements from an electro-optical sensor. This, while still a batch procedure, offers the flexibility of varying the batches depending on the estimation results.

8.2 Probabilistic Data Association

The PDA algorithm calculates in real-time the probability that each validated measurement is attributable to the target of interest. This probabilistic (Bayesian) information is used in a tracking filter, the PDA filter (PDAF), which accounts for the measurement origin uncertainty.

8.2.1 Assumptions

The following assumptions are made to obtain the recursive PDAF state estimator (tracker):

- There is only one target of interest whose state evolves according to a dynamic equation driven by process noise.
- The track has been initialized.
- The past information about the target is summarized approximately by

$$p\left[x(k)\middle|Z^{k-1}\right] = N\left[x(k); \hat{x}(k|k-1), P(k|k-1)\right] \tag{8.1}$$

where $N[x(k); \hat{x}(k|k-1)]$ denotes the normal probability density function (pdf) with argument $x(k)$, mean $\hat{x}(k|k-1)$, and covariance matrix $P(k|k-1)$. This assumption of the PDAF is similar to the GPB1 (Generalized Pseudo-Bayesian) approach,[10] where a single "lumped" state estimate is a quasi-sufficient statistic.

- At each time, a validation region as in Reference 3 is set up (see Equation 8.4).
- Among the possibly several validated measurements, at most one of them can be target-originated — if the target was detected and the corresponding measurement fell into the validation region.
- The remaining measurements are assumed to be false alarms or clutter and are modeled as independent identically distributed (iid) measurements with uniform spatial distribution.
- The target detections occur independently over time with known probability PD.

These assumptions enable a state estimation scheme to be obtained, which is almost as simple as the Kalman filter, but much more effective in clutter.

8.2.2 The PDAF Approach

The PDAF uses a decomposition of the estimation with respect to the origin of each element of the latest set of validated measurements, denoted as

$$Z(k) = \left\{ z_i(k) \right\}_{i=1}^{m(k)} \tag{8.2}$$

where $z_I(k)$ is the i-th validated measurement and $m(k)$ is the number of measurements in the validation region at time k.

The cumulative set (sequence) of measurements* is

$$Z^k = \left\{ Z(j) \right\}_{j=1}^{k} \tag{8.3}$$

8.2.3 Measurement Validation

From the Gaussian assumption (Equation 8.1), the validation region is the elliptical region

$$V(k,\gamma) = \left\{ Z: \left[z - \hat{z}(k|k-1) \right]' S(k)^{-1} \left[z - \hat{z}(k|k-1) \right] \le \gamma \right\} \tag{8.4}$$

where γ is the gate threshold and

$$S(k) = H(k) P(k|k-1) H(k)' + R(k) \tag{8.5}$$

is the covariance of the innovation corresponding to the true measurement. The volume of the validation region (Equation 8.4) is

$$V(k) = c_{n_z} \left| \gamma S(k) \right|^{1/2} = c_{n_z} \gamma^{\frac{n_z}{2}} \left| S(k) \right|^{1/2} \tag{8.6}$$

* When the running index is a time argument, a sequence exists; otherwise it is a set where the order is not relevant. The context should indicate which is the case.

where the coefficient c_{n_z} depends on the dimension of the measurement (it is the volume of the n_z-dimensional unit hypersphere: $c_1 = 2$, $c_2 = \pi$, $c_3 = 4\pi/3$, etc.).

8.2.4 The State Estimation

In view of the assumptions listed, the association events

$$\theta_i(k) = \begin{cases} \{z_i(k) \text{ is the target originated measurement}\} & i = 1,\ldots m(k) \\ \{\text{none of the measurements is target originated}\} & i = 0 \end{cases} \tag{8.7}$$

are mutually exclusive and exhaustive for $m(k) \geq 1$.

Using the total probability theorem[10] with regard to the above events, the conditional mean of the state at time k can be written as

$$\begin{aligned} \hat{x}(k|k) &= E\left[x(k)\middle|Z^k\right] \\ &= \sum_{i=0}^{m(k)} E\left[x(k)\middle|\theta_i(k), Z^k\right] P\left\{\theta_i(k)\middle|Z^k\right\} \\ &= \sum_{i=0}^{m(k)} \hat{x}_i(k|k)\beta_i(k) \end{aligned} \tag{8.8}$$

where $\hat{x}_i(k|k)$ is the updated state conditioned on the event that the i-th validated measurement is correct, and

$$\beta_i(k) \triangleq P\left\{\theta_i(k)\middle|Z_k\right\} \tag{8.9}$$

is the conditional probability of this event — the association probability, obtained from the PDA procedure presented in the next subsection.

The estimate conditioned on measurement i being correct is

$$\hat{x}_i(k|k) = \hat{x}(k|k-1) + W(k)v_i(k) \qquad i = 1,\ldots,m(k) \tag{8.10}$$

where the corresponding innovation is

$$v_i(k) = z_i(k) - \hat{z}(k|k-1) \tag{8.11}$$

The gain $W(k)$ is the same as in the standard filter

$$W(k) = P(k|k-1)H(k)'S(k)^{-1} \tag{8.12}$$

since, conditioned on $\theta_i(k)$, there is no measurement origin uncertainty.

For $i = 0$ (i.e., if none of the measurements is correct) or $m(k) = 0$ (i.e., there is no validated measurement)

$$\hat{x}_0(k|k) = \hat{x}(k|k-1) \tag{8.13}$$

8.2.5 The State and Covariance Update

Combining Equations 8.10 and 8.13 into Equation 8.8 yields the state update equation of the PDAF

$$\hat{x}(k|k) = \hat{x}(k|k-1) + W(k)v(k) \tag{8.14}$$

where the combined innovation is

$$v(k) = \sum_{i-1}^{m(k)} \beta_i(k) v_i(k) \tag{8.15}$$

The covariance associated with the updated state is

$$P(k|k) = \beta_0(k)P(k|k-1) + \left[1 - \beta_0(k)\right]P^c(k|k) + \tilde{P}(k) \tag{8.16}$$

where the covariance of the state updated with the correct measurement is[3]

$$P^c(k|k) = P(k|k-1) - W(k)S(k)W(k)' \tag{8.17}$$

and the spread of the innovations term (similar to the spread of the means term in a mixture[10]) is

$$\tilde{P}(k) \stackrel{\Delta}{=} W(k)\left[\sum_{i=1}^{m(k)} \beta_i(k) v_i(k) v_i(k)' - v(k)v(k)'\right] W(k)' \tag{8.18}$$

8.2.6 The Prediction Equations

The prediction of the state and measurement to k + 1 is done as in the standard filter, i.e.,

$$\hat{x}(k+1|k) = F(k)\hat{x}(k|k) \tag{8.19}$$

$$\hat{z}(k+1|k) = H(k+1)\hat{x}(k+1|k) \tag{8.20}$$

The covariance of the predicted state is, similarly,

$$P(k+1|k) = F(k)P(k|k)F(k)' + Q(k) \tag{8.21}$$

where $P(k|k)$ is given by Equation 8.16.

The innovation covariance (for the correct measurement) is, again, as in the standard filter

$$S(k+1) = H(k+1)P(k+1|k)H(k+1)' + R(k+1) \tag{8.22}$$

8.2.7 The Probabilistic Data Association

To evaluate the association probabilities, the conditioning is broken down into the past data Z^{k-1} and the latest data $Z(k)$. A probabilistic inference can be made on both the number of measurements in the validation region (from the clutter density, if known) and on their location, expressed as:

$$\beta_i(k) = P\left\{\theta_i(k) \middle| Z^k\right\} = P\left\{\theta_i(k) \middle| Z(k), m(k), Z^{k-1}\right\} \tag{8.23}$$

Using Bayes' formula, the above is rewritten as

$$\beta_i(k) = \frac{1}{c} p\left[Z(k) \middle| \theta_i(k), m(k), Z^{k-1}\right] p\left\{\theta_i(k) \middle| m(k), Z^{k-1}\right\} \qquad i = 0, \ldots, m(k) \tag{8.24}$$

The joint density of the validated measurements conditioned on $\theta_i(k)$, $i \neq 0$, is the product of

- The (assumed) Gaussian pdf of the correct (target-originated) measurements
- The pdf of the incorrect measurements, which are assumed to be uniform in the validation region whose volume $V(k)$ is given in Equation 8.6.

The pdf of the correct measurement (with the P_G factor that accounts for restricting the normal density to the validation gate) is

$$p\left[z_i(k) \middle| \theta_i(k), m(k), Z^{k-1}\right] = p_G^{-1} N\left[z_i(k); z(k|k-1), S(k)\right] = p_G^{-1} N\left[v_i(k); 0, S(k)\right] \tag{8.25}$$

The pdf from Equation 8.24 is then

$$p\left[Z(k) \middle| \theta_i(k), m(k), Z^{k-1}\right] = \left\{V(k)^{-m(k)+1} P_G^{-1} \mathcal{N}[\ ] \right. \tag{8.26}$$

The probabilities of the association events conditioned only on the number of validated measurements are

$$p\left[Z(k) \middle| \theta_i(k), m(k), Z^{k-1}\right] = \begin{cases} V(k)^{-m(k)+1} P_G^{-1} \mathcal{N}\left[v_i(k); 0, S(k)\right] & i = 1, \ldots, m(k) \\ V(k)^{-m(k)} & i = 0 \end{cases} \tag{8.27}$$

where $\mu_F(m)$ is the probability mass function (pmf) of the number of false measurements (false alarms or clutter) in the validation region.

Two models can be used for the pmf $\mu_F(m)$ in a volume of interest V:

1. A Poisson model with a certain spacial density λ

$$\mu_F(m) = e^{-\lambda V} \frac{(\lambda V)^m}{m!} \tag{8.28}$$

2. A diffuse prior model[3]

$$\mu_F(m) = \mu_F(m-1) = \delta \tag{8.29}$$

where the constant δ is irrelevant since it cancels out.

Using the (parametric) Poisson model in Equation 8.27 yields

$$\gamma_i\left[m(k)\right]=\begin{cases}P_D P_G\left[P_D P_G m(k)+\left(1-P_D P_G\right)\lambda V(k)\right]^{-1} & i=1,\ldots,m(k)\\ \left(1-P_D P_F\right)\lambda V(k)\left[P_D P_G m(k)+\left(1-P_D P_G\right)\lambda V(k)\right]^{-1} & i=0\end{cases} \tag{8.30}$$

The (nonparametric) diffuse prior (Equation 8.29) yields

$$\gamma_i\left[m(k)\right]=\begin{cases}\dfrac{1}{m(k)}P_D P_G & i=1,\ldots,m(k)\\ \left(1-P_D P_G\right) & i=0\end{cases} \tag{8.31}$$

The nonparametric model (Equation 8.31) can be obtained from Equation 8.30 by setting

$$\lambda=\frac{m(k)}{V(k)} \tag{8.32}$$

i.e., replacing the Poisson parameter with the sample spatial density of the validated measurements. The volume $V(k)$ of the elliptical (i.e., Gaussian-based) validation region is given in Equation 8.6.

8.2.8 The Parametric PDA

Using Equations 8.30 and 8.26 with the explicit expression of the Gaussian pdf in Equation 8.24 yields, after some cancellations, the final equations of the parametric PDA with the Poisson clutter model

$$\beta_i(k)=\begin{cases}\dfrac{e_i}{b+\sum_{j=1}^{m(k)} e_j} & i=1,\ldots,m(k)\\ \dfrac{b}{b+\sum_{j=1}^{m(k)} e_j} & i=0\end{cases} \tag{8.33}$$

where

$$e_i\triangleq e^{-\frac{1}{2}v_i(k)'S(k)^{-1}v_i(k)} \tag{8.34}$$

$$b\triangleq\lambda\left|2\pi S(k)\right|^{1/2}\frac{1-P_D P_G}{P_D} \tag{8.35}$$

The last expression above can be rewritten as

$$b=\left(\frac{2\pi}{\lambda}\right)^{\frac{n_z}{2}}\lambda V(k)c_{n_z}^{-1}\frac{1-P_D P_G}{P_D} \tag{8.36}$$

8.2.9 The Nonparametric PDA

The nonparametric PDA is the same as above except for replacing $\lambda V(k)$ in Equation 8.36 by $m(k)$ — this obviates the need to know λ.

8.3 Low Observable TMA Using the ML-PDA Approach with Features

This section considers the problem of target motion analysis (TMA) — estimation of the trajectory parameters of a constant velocity target — with a passive sonar, which does not provide full target position measurements. The methodology presented here applies equally to any *target motion characterized by a deterministic equation*, in which case the initial conditions (a finite dimensional parameter vector) characterize in full *the entire motion*. In this case the (batch) maximum likelihood (ML) parameter estimation can be used; this method is more powerful than state estimation when the target motion is deterministic (it does not have to be linear). Furthermore, the ML-PDA approach makes no approximation, unlike the PDAF in Equation 8.1.

8.3.1 Amplitude Information Feature

The standard TMA consists of estimating the target's position and its constant velocity from bearings-only (wideband sonar) measurements corrupted by noise.[10] Narrowband passive sonar tracking, where frequency measurements are also available, has been studied.[11] The advantages of narrowband sonar are that it does not require a maneuver of the platform for observability, and it greatly enhances the accuracy of the estimates. However, not all passive sonars have frequency information available. In both cases, the intensity of the signal at the output of the signal processor, which is referred to as *measurement amplitude* or *amplitude information* (AI), is used implicitly to determine whether there is a valid measurement. This is usually done by comparing it with the detection threshold, which is a design parameter.

This section shows that the measurement amplitude carries valuable information and that its use in the estimation process increases the observability even though the amplitude information cannot be correlated to the target state directly. Also superior global convergence properties are obtained.

The pdf of the envelope detector output (i.e., the AI) a when the signal is due to noise only is denoted as $p_0(a)$ and the corresponding pdf when the signal originated from the target is $p_1(a)$. If the signal-to-noise ratio (SNR — this is the SNR in a resolution cell, to be denoted later as SNR_c) is d, the density functions of noise only and target-originated measurements can be written as

$$p_0(a) = a \exp\left(-\frac{a^2}{2}\right) \quad a \geq 0 \tag{8.37}$$

$$p_1(a) = \frac{a}{1+d} \exp\left(-\frac{a^2}{2(1+d)}\right) \quad a \geq 0 \tag{8.38}$$

respectively. This is a Rayleigh fading amplitude (Swerling I) model believed to be the most appropriate for shallow water passive sonar.

A suitable threshold, denoted by τ, is used to declare a detection. The probability of detection and the probability of false alarm are denoted by P_D and P_{FA}, respectively. Both P_D and P_{FA} can be evaluated from the probability density functions of the measurements. Clearly, in order to increase P_D, the threshold τ must be lowered. However, this also increases P_{FA}. Therefore, depending on the SNR, τ must be selected to satisfy two conflicting requirements.*

The density functions given above correspond to the signal at the envelope detector output. Those corresponding to the output of the threshold detector are

*For other probabilistic models of the detection process, different SNR values correspond to the same P_D, P_{FA} pair. Compared to the Rician model receiver operating characteristic (ROC) curve, the Rayleigh model ROC curve requires a higher SNR for the same pair (P_D, P_{FA}), i.e., the Rayleigh model considered here is pessimistic.

$$\rho_0^{\tau}(a) = \frac{1}{P_{FA}} p_0(a) = \frac{1}{P_{FA}} a \exp\left(-\frac{a^2}{2}\right) \quad a > \tau \tag{8.39}$$

$$\rho_1^{\tau}(a) = \frac{1}{P_D} p_1(a) = \frac{1}{P_D} \frac{a}{1+d} a \exp\left(-\frac{a^2}{2(1+d)}\right) \quad a > \tau \tag{8.40}$$

where $\rho_0^{\tau}(a)$ is the pdf of the validated measurements that are caused by noise only, and $\rho_1^{\tau}(a)$ is the pdf of those that originated from the target. In the following, a is the amplitude of the candidate measurements. The amplitude likelihood ratio, ρ, is defined as

$$\rho = \frac{p_1^{\tau}(a)}{p_0^{\tau}(a)} \tag{8.41}$$

8.3.2 Target Models

Assume that n sets of measurements, made at times $t = t_1, t_2, \ldots, t_n$, are available.

For bearings-only estimation, the target motion is defined by the four-dimensional parameter vector

$$x \stackrel{\Delta}{=} \left[\xi(t_0),\ \eta(t_0),\ \dot{\xi},\ \dot{\eta}\right] \tag{8.42}$$

where $\xi(t_0)$ and $\eta(t_0)$ are the distances of the target in the east and north directions, respectively, from the origin at the reference time t_0. The corresponding velocities, assumed constant, are $\dot{\xi}$ and $\dot{\eta}$, respectively. This assumes deterministic target motion (i.e., no process noise[10]). Any other deterministic motion (e.g., constant acceleration) can be handled within the same framework.

The state of the platform at t_i $(i = 1, \ldots, n)$ is defined by

$$x_p(t_i) \stackrel{\Delta}{=} \left[\xi_p(t_i),\ \eta_p(t_i),\ \dot{\xi}_p(t_i),\ \dot{\eta}_p(t_i)\right]' \tag{8.43}$$

The relative position components in the east and north directions of the target with respect to the platform at t_i are defined by $r_\xi(t_i, x)$ and $r_\eta(t_i, x)$, respectively. Similarly, $v_\xi(t_i, x)$ and $v_\eta(t_i, x)$ define the relative velocity components. The true bearing of the target from the platform at t_i is given by

$$\theta_i(x) \stackrel{\Delta}{=} \tan^{-1}\left[r_\xi(t_i, x) / r_\eta(t_i, x)\right] \tag{8.44}$$

The range of possible bearing measurements is

$$U_\theta \stackrel{\Delta}{=} \left[\theta_1, \theta_2\right] \subset \left[0, 2\pi\right] \tag{8.45}$$

The set of measurements at t_i is denoted by

$$Z(i) \stackrel{\Delta}{=} \left\{z_j(i)\right\}_{j=1}^{m_i} \tag{8.46}$$

where m_i is the number of measurements at t_i, and the pair of bearing and amplitude measurements $z_j(i)$, is defined by

$$z_j(i) \triangleq \left[\beta_{ij} \quad a_{ij}\right]' \tag{8.47}$$

The cumulative set of measurements during the entire period is

$$Z^n \triangleq \left\{Z(i)\right\}_{i=1}^{n} \tag{8.48}$$

The following additional assumptions about the statistical characteristics of the measurements are also made:[11]

1. The measurements at two different sampling instants are conditionally independent, i.e.,

$$p\left[Z(i_1), Z(i_2)\middle| x\right] = p\left[Z(i_1)\middle| x\right] p\left[Z(i_2)\middle| x\right] \quad \forall i_1 \neq i_2 \tag{8.49}$$

   where $p[\cdot]$is the probability density function.
2. A measurement that originated from the target at a particular sampling instant is received by the sensor only once during the corresponding scan with probability P_D and is corrupted by zero-mean Gaussian noise of known variance. That is

$$\beta_{ij} = \theta_i(x) + \in_{ij} \tag{8.50}$$

   where $\in_{ij} \sim \mathcal{N}\left[0, \sigma_\theta^2\right]$ is the bearing measurement noise. Due to the presence of false measurements, the index of the true measurement is not known.
3. The false bearing measurements are distributed uniformly in the surveillance region, i.e.,

$$\beta_{ij} \sim \mathcal{U}\left[\theta_1, \theta_2\right] \tag{8.51}$$

4. The number of false measurements at a sampling instant is generated according to a Poisson law with a known expected number of false measurements in the surveillance region. This is determined by the detection threshold at the sensor (exact equations are given in Section 8.3.5).

For narrowband sonar (with frequency measurements) the target motion model is defined by the five-dimensional vector

$$x \triangleq \left[\xi(t_1), \quad \eta(t_1), \quad \dot{\xi}, \quad \dot{\eta}, \quad \gamma\right] \tag{8.52}$$

where γ is the unknown emitted frequency assumed constant. Due to the relative motion between the target and platform at t_i, this frequency will be Doppler shifted at the platform. The (noise-free) shifted frequency, denoted by $\gamma_i(x)$, is given by

$$\gamma_i(x) = \gamma\left[1 - \frac{v_\xi(t_i, x)\sin\theta_i(x) + v_n(t_i, x)\cos\theta_i(x)}{c}\right] \tag{8.53}$$

where c is the velocity of sound in the medium. If the bandwidth of the signal processor in the sonar is $[\Omega_1, \Omega_2]$, the measurements can lie anywhere within this range. As in the case of bearing measurements,

we assume that an operator is able to select a frequency subregion $[\Gamma_1, \Gamma_2]$ for scanning. In addition to the bearing surveillance region given in Equation 8.45, the region for frequency is defined as

$$U_\gamma \triangleq \left[\Gamma_1, \Gamma_2\right] \subset \left[\Omega_1, \Omega_2\right] \tag{8.54}$$

The noisy frequency measurements are denoted by f_{ij} and the measurement vector is

$$z_j(i) \triangleq \left[\beta_{ij},\ \ f_{ij},\ \ a_{ij}\right]' \tag{8.55}$$

As for the statistical assumptions, those related to the conditional independence of measurements (assumption 1) and the number of false measurements (assumption 4) are still valid. The equations relating the number of false alarms in the surveillance region to detection threshold are given in Section 8.3.5.

The noisy bearing measurements satisfy Equation 8.50 and the noisy frequency measurements f_{ij} satisfy

$$f_{ij} = \gamma_i(x) + \nu_{ij} \tag{8.56}$$

where $\nu_{ij} \sim \mathcal{N}\left[0, \sigma_\gamma^2\right]$ is the frequency measurement noise.

It is also assumed that these two measurement noise components are conditionally independent. That is,

$$p\left(\in_{ij}, \nu_{ij} \middle| x\right) = p\left(\in_{ij} \middle| x\right) p\left(\nu_{ij} \middle| x\right) \tag{8.57}$$

The measurements resulting from noise only are assumed to be uniformly distributed in the entire surveillance region.

8.3.3 Maximum Likelihood Estimator Combined with PDA — The ML-PDA

In this section we present the derivation and implementation of the maximum likelihood estimator combined with the PDA technique for both bearings-only tracking and narrowband sonar tracking. If there are m_i detections at t_i, one has the following mutually exclusive and exhaustive events:[3]

$$\varepsilon_j(i) \triangleq \begin{cases} \left\{\text{measurement } z_j(i) \text{ is from the target}\right\} & j = 1, \ldots, m_i \\ \left\{\text{all measurements are false}\right\} & j = 0 \end{cases} \tag{8.58}$$

The pdf of the measurements corresponding to the above events can be written as

$$p\left(Z(i) \middle| e_j(i), x\right) = \begin{cases} u^{1-m_i} p\left(\beta_{ij}\right) \rho_{ij} \prod_{j=1}^{m_i} p_0^\tau\left(a_{ij}\right) & j = 1, \ldots, m_i \\ u^{-m_i} \prod_{j=1}^{m_i} p_0^\tau\left(a_{ij}\right) & j = 0 \end{cases} \tag{8.59}$$

where $u = U_\theta$ is the area of the surveillance region.

Using the total probability theorem, the likelihood function of the set of measurements at t_i can be expressed as

$$p\left[Z(i)\middle|x\right] = u^{-m_i}\left(1-P_D\right)\prod_{j=1}^{m_i} p_0^{\tau}\left(a_{ij}\right)\mu_f\left(m_i\right) + \frac{u^{1-m_i}P_D\mu_f\left(m_i-1\right)}{m_i}\prod_{j=1}^{m_i} p_0^{\tau}\left(a_{ij}\right)\sum_{j=1}^{m_i} p\left(b_{ij}\right)\rho_{ij}$$

$$= u^{-m_i}\left(1-P_D\right)\prod_{j=1}^{m_i} p_0^{\tau}\left(a_{ij}\right)\mu_f\left(m_i\right) + \frac{u^{1-m_i}P_D\mu_f\left(m_i-1\right)}{m_i}\prod_{j=1}^{m_i} p_0^{\tau}\left(a_{ij}\right) \tag{8.60}$$

$$\cdot\sum_{j=1}^{m_i}\frac{1}{\sqrt{2\pi\sigma_\theta}}\exp\left(-\frac{1}{2}\left[\frac{\beta_{ij}-\theta_i\left(x\right)}{\sigma_\theta}\right]^2\right)\rho_{ij}$$

where $\mu_f(m_i)$ is the Poisson probability mass function of the number of false measurements at t_i. Dividing the above by $p[Z(I)|\varepsilon_0(I), x]$ yields the *dimensionless* likelihood ratio $\Phi_i[Z(I), x]$ at t_i. Then

$$\Phi_i\left[Z(i),x\right] = \frac{p\left[Z(i),x\right]}{p\left[Z(i)\middle|\varepsilon_0(i),x\right]}$$

$$= \left(1-P_D\right) + \frac{P_D}{\lambda}\sum_{j=1}^{m_i}\frac{1}{\sqrt{2\pi\sigma_\theta}}\rho_{ij}\exp\left(-\frac{1}{2}\left[\frac{\beta_{ij}-\theta_i\left(x\right)}{\sigma_\theta}\right]^2\right) \tag{8.61}$$

where λ is the expected number of false alarms per unit area. Alternately, the log-likelihood ratio at t_i can be defined as

$$\phi_i\left[Z(i),x\right] = \ln\left[\left(1-P_D\right) + \frac{P_D}{\lambda}\sum_{j=1}^{m_i}\frac{1}{\sqrt{2\pi\sigma_\theta}}\rho_{ij}\exp\left(-\frac{1}{2}\left[\frac{\beta_{ij}-\theta_i\left(x\right)}{\sigma_\theta}\right]^2\right)\right] \tag{8.62}$$

Using conditional independence of measurements, the likelihood function of the entire set of measurements can be written in terms of the individual likelihood functions as

$$p\left[Z^n\middle|x\right] = \prod_{i=1}^{n} p\left[Z(i)\middle|x\right] \tag{8.63}$$

Then the dimensionless likelihood ratio for the entire data is given by

$$\Phi\left[Z^n,x\right] = \prod_{i=1}^{n}\Phi_i\left[Z(i),x\right] \tag{8.64}$$

From the above, the total log-likelihood ratio $\Phi_i[Z(i), x]t_i$ can be expressed as

$$\Phi\left[Z^n,x\right] = \sum_{i=1}^{n}\ln\left[\left(1-P_D\right) + \frac{P_D}{\lambda}\sum_{j=1}^{m_i}\frac{1}{\sqrt{2\pi\sigma_\theta}}\rho_{ij}\exp\left(-\frac{1}{2}\left[\frac{\beta_{ij}-\theta_i\left(x\right)}{\sigma_\theta}\right]^2\right)\right] \tag{8.65}$$

The maximum likelihood estimate (MLE) is obtained by finding the state $x = \hat{x}$ that maximizes the total log-likelihood function. In deriving the likelihood function, the gate probability mass, which is the probability that a target-originated measurement falls within the surveillance region, is assumed to be one. The operator selects the appropriate region.

Arguments similar to those given earlier can be used to derive the MLE when frequency measurements are also available. Defining $\varepsilon_j(i)$ as in Equation 8.58, the pdf of the measurements is

$$p\left[Z(i)\middle|\varepsilon_j(i),x\right]=\begin{cases}u^{1-m_i}p(\beta_{ij})p(f_{ij})p_{ij}\prod_{j=1}^{m_i}p_0^{\tau}(a_{ij}) & j=1,\ldots,m_i\\ u^{-m_i}\prod_{j=1}^{m_i}p_0^{\tau}(a_{ij}) & j=0\end{cases} \tag{8.66}$$

where $u = U_\theta U_\gamma$ is the volume of the surveillance region.

After some lengthy manipulations, the total log-likelihood function is obtained as

$$\phi\left[Z^n,x\right]=\sum\ln\left[(1-P_D)+\frac{P_D}{\lambda}\sum_{j=1}^{m_i}\frac{\rho_{ij}}{2\pi\sigma_\theta\sigma_\gamma}\exp\left(-\frac{1}{2}\left[\frac{\beta_{ij}-\theta_i(x)}{\sigma_\theta}\right]^2-\frac{1}{2}\left[\frac{f_{ij}-\gamma_i(x)}{\sigma_\gamma}\right]^2\right)\right] \tag{8.67}$$

For narrowband sonar, the MLE is found by maximizing Equation 8.67.

This section demonstrated the essence of the use of the PDA — all the measurements are accounted for and the likelihood function is evaluated using the total probability theorem, similar to Equation 8.8. However, since Equation 8.67 is *exact* (for the parameter estimation formulation), there is no need for the approximation in Equation 8.1, which is necessary in the PDAF for state estimation.

The same ML-PDA approach is applicable to the estimation of the trajectory of an exoatmospheric ballistic missile.[12,13] The modification of this fixed-batch ML-PDA estimator to a flexible (sliding/expanding/contracting) procedure is discussed in Section 8.5 and demonstrated with an actual electro-optics (EO) data example.

8.3.4 Cramér-Rao Lower Bound for the Estimate

For an unbiased estimate, the Cramér-Rao lower bound (CRLB) is given by

$$E\left\{(x-\hat{x})(x-\hat{x})'\right\}\geq J^{-1} \tag{8.68}$$

where J is the Fisher information matrix (FIM) given by

$$J=E\left\{\left[\nabla_x\ln p\left(Z^n\middle|x\right)\right]\left[\nabla_x\ln p\left(Z^n\middle|x\right)\right]'\right\}\Big|_{x=x_{true}} \tag{8.69}$$

Only in simulations will the true value of the state parameter be available. In practice CRLB is evaluated at the estimate.

As expounded in Reference 14, the FIM J is given in the present ML-PDA approach for the bearings-only case — *wideband sonar* — by

$$J=q_2\left(P_D,\lambda\nu_g,g\right)\sum_{i=1}^{n}\frac{1}{\sigma_\theta^2}\left[\nabla_x\theta_i(x)\right]\left[\nabla x\theta i(x)\right]' \tag{8.70}$$

where $q_2(P_D, \lambda v_g, g)$ is the *information reduction factor* that accounts for the loss of information resulting from the presence of false measurements and less-than-unity probability of detection,[3] and the expected number of false alarms per unit volume is denoted by λ.

In deriving Equation 8.70, only the bearing measurements that fall within the validation region

$$V_g^i(x) \triangleq \left\{ \beta_{ij} : \left| \frac{\beta_{ij} - \theta_i(x)}{\sigma_\theta} \right| \le g \right\} \tag{8.71}$$

at t_i were considered. The validation region volume (g-sigma region), v_g, is given by

$$v_g = 2\sigma_\theta g \tag{8.72}$$

The information reduction factor $q_2(P_D, \lambda v_g, g)$ for the present two-dimensional measurement situation (bearing *and* amplitude) is given by

$$q_2(P_D, \lambda v_g, g) = \frac{1}{1+d} \sqrt{\frac{2}{\pi}} \sum_{m=1}^{\infty} \frac{\mu_f(m-1)}{(gP_{FA})^{m-1}} I_2(m, P_D, g) \tag{8.73}$$

where $I_2(m, P_D, g)$ is a $2m$-fold integral given in Reference 14 where numerical values of $q_2(P_D, \lambda v_g, g)$ for different combinations of P_D and λv_g are also presented. The derivation of the integral is based on Bar-Shalom and Li.[3] In this implementation, $g = 5$ was selected. Knowing P_D and λv_g, P_{FA} can be determined by using

$$\lambda v_g = P_{FA} \frac{v_g}{V_c} \tag{8.74}$$

where V_c is the resolution cell volume of the signal processor (discussed in more detail in Section 8.3.5). Finally, d, the SNR, can be calculated from P_D and λv_g.

The rationale for the term *information reduction factor* follows from the fact that the FIM for zero false alarm probability and unity target detection probability, J_0, is given by Reference 10

$$J_0 = \sum_{i=1}^{n} \frac{1}{\sigma_\theta^2} [\nabla_x \theta_i(x)][\nabla_x \theta_i(x)]' \tag{8.75}$$

Equations 8.70 and 8.75 clearly show that $q_2(P_D, \lambda v_g, g)$, which is always less than or equal to unity, represents the loss of information due to clutter.

For *narrowband sonar* (bearing and frequency measurements), the FIM is given by

$$J = q_2(P_D, \lambda v_g, g) \sum_{i=1}^{n} \left\{ \frac{1}{\sigma_\theta^2} [\nabla_x \theta_i(x)][\nabla_x \theta_i(x)]' + \frac{1}{\sigma_\theta^2} [\nabla_x \gamma_i(x)][\nabla_x \gamma_i(x)]' \right\} \tag{8.76}$$

where $q_2(P_D, \lambda v_g, g)$ for this three-dimensional measurement (bearing, frequency, and amplitude) case is evaluated[14] using

$$q_2(P_D, \lambda v_g, g) = \frac{1}{1+d} \sum \frac{2^{m-1} \mu_f(m-1)}{(g^2 P_{FA})^{m-1}} I_2(m, P_D, g) \tag{8.77}$$

The expression for $I_2(m, P_D, g)$ and the numerical values for $q_2(P_D, \lambda v_g, g)$ are also given by Kirubarajan and Bar-Shalom.[14]

For narrowband sonar, the validation region is defined by

$$V_g^i(x) \triangleq \left\{ (\beta_{ij}, f_{ij}) : \left[\frac{\beta_{ij} - \theta_i(x)}{\sigma_\theta} \right]^2 + \left[\frac{f_{ij} - \theta_i(x)}{\sigma\gamma} \right]^2 \right\} \leq g^2 \tag{8.78}$$

and the volume of the validation region, v_g, is

$$v_g = \sigma^\theta \sigma^\gamma g^2 \tag{8.79}$$

8.3.5 Results

Both the bearings-only and narrowband sonar problems with amplitude information were implemented to track a target moving at constant velocity. The results for the narrowband case are given below, accompanied by a discussion of the advantages of using amplitude information by comparing the performances of the estimators with and without amplitude information.

In narrowband signal processing, different bands in the frequency domain are defined by an appropriate cell resolution and a center frequency about which these bands are located. The received signal is sampled and filtered in these bands before applying FFT and beamforming. Then the angle of arrival is estimated using a suitable algorithm.[15] As explained earlier, the received signal is registered as a valid measurement only if it exceeds the threshold τ. The threshold value, together with the SNR, determines the probability of detection and the probability of false alarm.

The signal processor was assumed to consist of the frequency band [500Hz, 1000Hz] with a 2048-point FFT. This results in a frequency cell whose size is given by

$$C_\gamma = 500/2048 \approx 0.25\text{Hz} \tag{8.80}$$

Regarding azimuth measurements, the sonar is assumed to have 60 equal beams, resulting in an azimuth cell C_θ with size

$$C_\theta = 180°/60 = 3.0° \tag{8.81}$$

Assuming uniform distribution in a cell, the frequency and azimuth measurement standard deviations are given by*

$$\sigma_\gamma = 0.25/\sqrt{12} = 0.0722\text{Hz} \tag{8.82}$$

$$\sigma_\theta = 3.0/\sqrt{12} = 0.866° \tag{8.83}$$

The SNR_C in a cell** was taken as 6.1dB and $P_D = 0.5$. The estimator is not very sensitive to an incorrect P_D.This is verified by running the estimator with an incorrect P_D on the data generated with a different

* The "uniform" factor $\sqrt{12}$ corresponds to the worst case. In practice, σ_θ and σ_γ are functions of the 3dB-bandwidth and of the SNR.

** The commonly used SNR, designated here as SNR_1, is signal strength divided by the noise power in a 1-Hz bandwidth. SNR_C is signal strength divided by the noise power in a resolution cell. The relationship between them, for $C_\gamma = 0.25$Hz is $\text{SNR}_C = \text{SNR}_1 - 6$dB. SNR_C is believed to be the more meaningful SNR because it determines the ROC curve.

P_D. Differences up to 0.15 are tolerated by the estimator. The corresponding SNR in a 1-Hz bandwidth SNR_1 is 0.1dB. These values give

$$\tau = 2.64 \tag{8.84}$$

$$P_{FA} = 0.306 \tag{8.85}$$

From P_{FA}, the expected number of false alarms per unit volume, denoted by λ, can be calculated using

$$P_{FA} = \lambda C_\theta C_\gamma \tag{8.86}$$

Substituting the values for C_θ and λ gives

$$\lambda = \frac{0.0306}{3.0 \times 0.25} = 0.0407/\deg \cdot \text{Hz} \tag{8.87}$$

The surveillance regions for azimuth and frequency, denoted by U_θ and U_γ, respectively, are taken as

$$U_\theta = \left[-20°, 20°\right] \tag{8.88}$$

$$U_\gamma = \left[747\text{Hz}, 753\text{Hz}\right] \tag{8.89}$$

The expected number of false alarms in the entire surveillance region and that in the validation gate V_g can be calculated. These values are 9.8 and 0.2, respectively, where the validation gate is restricted to $g = 5$. These values mean that, for every true measurement that originated from the target, there are about 10 false alarms that exceed the threshold.

The estimated tracks were validated using the hypothesis testing procedure described in Reference 14. The track acceptance test was carried out with a miss probability of five percent.

To check the performance of the estimator, simulations were carried out with clutter only (i.e., without a target) and also with a target present; measurements were generated accordingly. Simulations were done in batches of 100 runs.

When there was no target, irrespective of the initial guess, the estimated track was always rejected. This corroborates the accuracy of the validation algorithm given by Kirubarajan and Bar-Shalom.[14]

For the set of simulations with a target, the following scenario was selected: the target moves at a speed of 10 m/s heading west and 5 m/s heading north starting from (5000 m, 35,000 m). The signal frequency is 750 Hz. The target parameter is x = [5000 m, 35,000 m, –10 m/s, 5 m/s, 750 Hz]. The motion of the platform consisted of two velocity legs in the northwest direction during the first half, and in the northeast direction during the second half of the simulation period with a constant speed of 7:1 m/s. Measurements were taken at regular intervals of 30 s. The observation period was 900 s. Figure 8.1 shows the scenario including the target true trajectory (solid line), platform trajectory (dashed line), and the 95% probability regions of the position estimates at the initial and final sampling instants based on the CRLB (Equation 8.76). The initial and the final positions of the trajectories are marked by I and F, respectively. The purpose of the probability region is to verify the validity of the CRLB as the actual parameter estimate covariance matrix from a number of Monte Carlo runs.[4]

Figure 8.1 shows the 100 tracks formed from the estimates. Note that in all but six runs (i.e., 94 runs) the estimated trajectory endpoints fall in the corresponding 95% uncertainty ellipses.

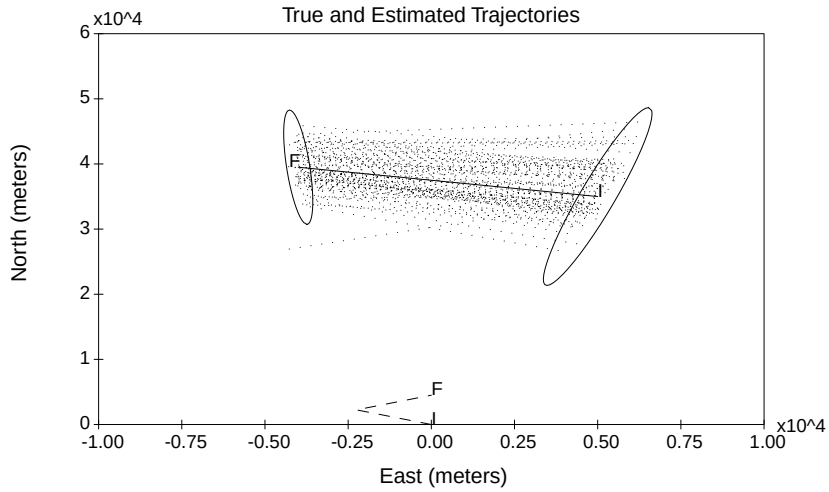

FIGURE 8.1 Estimated tracks from 100 runs for narrowband sonar with AI.

TABLE 8.1 Results of 100 Monte Carlo Runs for Narrowband Sonar with AI (SNRC = 6:1dB)

Unit	x_{true}	x_{init}	$\bar{x}$	σ_{CRLB}	$\hat{\sigma}$
m	5000	–12,000 to 12,000	4991	667	821
m	35,000	49,000 to 50,000	35,423	5576	5588
m/s	–10	–16 to 5	–9.96	0.85	0.96
m/s	5	–4 to 9	4.87	4.89	4.99
Hz	750	747 to 751	749.52	2.371	2.531

Table 8.1 gives the numerical results from 100 runs. Here $\bar{x}$ is the average of the estimates, $\hat{\sigma}$ the variance of the estimates evaluated from 100 runs, and σ_{CRLB} the theoretical CRLB derived in Section 8.3.4. The range of initial guesses found by rough grid search to start off the estimator are given by x_{init}.

The efficiency of the estimator was verified using the normalized estimation error squared (NEES)[10] defined by

$$\in_x \triangleq \left(x-\hat{x}\right)' J\left(x-\hat{x}\right) \tag{8.90}$$

where $\bar{x}$ is the estimate, and J is the FIM (Equation 8.76). Assuming approximately Gaussian estimation error, the NEES is chi-square distributed with n degrees-of-freedom where n is the number of estimated parameters. For the 94 accepted tracks the NEES obtained was 5.46, which lies within the 95% confidence region [4:39; 5:65]. Also note that each component of $\bar{x}$ is within $2\hat{\sigma}/\sqrt{100}$ of the corresponding component of x_{true}.

8.4 The IMMPDAF for Tracking Maneuvering Targets

Target tracking is a problem that has been well studied and documented. Some specific problems of interest in the single-target, single-sensor case are tracking maneuvering targets,[10] tracking in the presence of clutter,[3] and electronic countermeasures (ECM). In addition to these tracking issues, a complete

tracking system for a sophisticated electronically steered antenna radar has to consider radar scheduling, waveform selection, and detection threshold selection.

Although many researchers have worked on these issues and many algorithms are available, there had been no standard problem comparing the performances of the various algorithms. Rectifying this, the first benchmark problem[16] was developed, focusing only on tracking a maneuvering target and pointing/scheduling a phased array radar. Of all the algorithms considered for this problem, the interacting multiple model (IMM) estimator yielded the best performance.[17] The second benchmark problem[9] included false alarms (FA) and ECM — specifically, a stand-off jammer (SOJ) and range gate pull off (RGPO) — as well as several possible radar waveforms (from which the resource allocator has to select one at every revisit time). Preliminary results for this problem showed that the IMM and multiple-hypothesis tracking (MHT) algorithms were the best solutions.[6,9] For the problem considered, the MHT algorithm yielded similar results as the IMM estimator with probabilistic data association filter (IMMPDAF) modules,[3] although the MHT algorithm was one to two orders of magnitude costlier computationally (as many as 40 hypotheses were needed*). The benchmark problem of Reference 18 was upgraded in Reference 8 to require the radar resource allocator/manager to select the operating constant false alarm rate (CFAR) and included the effects of the SOJ on the direction of arrival (DOA) measurements; also the SOJ power was increased to present a more challenging benchmark problem. While, in Reference 18, the primary performance criterion for the tracking algorithm was minimization of radar energy, the primary performance was changed in Reference 8 to minimization of a weighted combination of radar time and energy.

This section presents the IMMPDAF technique for automatic track formation, maintenance, and termination. The coordinate selection for tracking, radar scheduling/pointing and the models used for mode-matched filtering (the modules inside the IMM estimator) are also discussed. These cover the target tracking aspects of the solution to the benchmark problem. These are based on the benchmark problem tracking and sensor resource management.[6,8]

8.4.1 Coordinate Selection

For target tracking in track-dwell mode of the radar, the number of detections at scan k (time t_k) is denoted by m_k. The m-th detection report $\bar{\zeta}_m(t_k)$ ($m = 1,2,\ldots,m_k$) consists of a time stamp t_k, range r_m, bearing b_m, elevation e_m, amplitude information (AI) ρ_m given by the SNR, and the standard deviations of bearing and elevation measurements, σ_m^b and σ_m^e, respectively. Thus,

$$\bar{\zeta}_m(t_k) = \left[t_k,\ r_m,\ b_m,\ e_m,\ \rho_m,\ \sigma_m^b,\ \sigma_m^e\right]' \tag{8.91}$$

where the overbar indicates that this is in the radar's spherical coordinate system.

The AI is used only to declare detections and select the radar waveform for the next scan. Since the use of AI, for example, as in Reference 17, can be counterproductive in discounting RGPO measurements, which generally have higher SNR than target-originated measurements, AI is not utilized in the estimation process itself. Using the AI would require a separate model for the RGPO intensity, which cannot be estimated in real time due to its short duration and variability.[17]

For target tracking, the measurements are converted from spherical coordinates to Cartesian coordinates, and then the IMMPDAF is used on these converted measurements. This conversion avoids the use of extended Kalman filters and makes the problem linear.[4] The converted measurement report $\zeta_m(t_k)$ corresponding to $\bar{\zeta}_m(t_k)$ is given by[6]

$$\zeta_m(t_k) = \left[t_k,\ x_m,\ y_m,\ z_m,\ \rho_m,\ R_m\right] \tag{8.92}$$

* The more recent IMM-MHT (as opposed to Kalman filter-based MHT) requires six to eight hypotheses.

where x_m, y_m, z_m, and R_m are the three position measurements in the Cartesian frame and their covariance matrix, respectively. The converted values are

$$x_m = r_m \cos\left(b_m\right)\cos\left(e_m\right) \tag{8.93}$$

$$y_m = r_m \sin\left(b_m\right)\cos\left(e_m\right) \tag{8.94}$$

$$z_m = r_m \sin\left(e_m\right) \tag{8.95}$$

$$R_m = T_m \cdot diag\left[\left(\sigma_k^r\right)^2, \left(\sigma_m^b\right)^2, \left(\sigma_m^e\right)^2\right] \cdot T_m' \tag{8.96}$$

where σ_k^r is the standard deviation of range measurements at scan k and T_m is the spherical-to-Cartesian transformation matrix given by

$$T_m = \begin{bmatrix} \cos\left(b_m\right)\cos\left(e_m\right) & -r_m \sin\left(b_m\right)\cos\left(e_m\right) & -r_m \cos\left(b_m\right)\cos\left(e_m\right) \\ \sin\left(b_m\right)\cos\left(e_m\right) & r_m \cos\left(b_m\right)\cos\left(e_m\right) & -r_m \sin\left(b_m\right)\cos\left(e_m\right) \\ \sin\left(e_m\right) & 0 & r_m \cos\left(e_m\right) \end{bmatrix} \tag{8.97}$$

For the scenarios considered here, this transformation is practically unbiased and there is no need for the debiasing procedure of Reference 4.

8.4.2 Track Formation

In the presence of false alarms, track formation is crucial. Incorrect track initiation will result in target loss. In Reference 3, an automatic track formation/deletion algorithm in the presence of clutter is presented based on the IMM algorithm. In the present benchmark problem, a noisy measurement corresponding to the target of interest is given in the first scan.* Forming new tracks for each validated measurement (based on a velocity gate) at subsequent scans, as suggested in Reference 3 and as implemented in Reference 6, is expensive in terms of both radar energy and computational load. In this implementation, track formation is simplified and handled as follows:

Scan 1 (t = 0s) — As defined by the benchmark problem, there is only one (target-originated, noisy) measurement. The position component of this measurement is used as the starting point for the estimated track.

Scan 2 (t = 0.1s) — The beam is pointed at the location of the first measurement. This yields, possibly, more than one measurement and these measurements are gated using the maximum possible velocity of the targets to avoid the formation of impossible tracks. This validation region volume, which is centered on the initial measurement, is given by

$$V_{xyz} = \left[2\left(\dot{x}_{\max}\delta_2 + 3\sqrt{R_{m_2}^x}\right)\right]\left[2\left(y_{\max}\delta_2 + 3\sqrt{R_{m_2}^y}\right)\right]\left[2\left(z_{\max}\delta_2 + 3\sqrt{R_{m_2}^z}\right)\right] \tag{8.98}$$

where δ_2 = 0:1s is the sampling interval and $\dot{x}_{\max}\delta_2$, $y_{\max}\delta_2$, and $z_{\max}\delta_2$ are the maximum speeds in the X, Y, and Z directions respectively; $R_{m_2}^x$, $R_{m_2}^y$, and $R_{m_2}^z$ are the variances of position measurements in these directions obtained from the diagonal components of Equation 8.96. The maximum speed in each direction is assumed to be 500 m/s.

*Assuming that this is a search pulse without (monopulse) split-beam processing, the angular errors are uniformly distributed in the beam.

The measurement in the first scan and the measurement with the highest SNR in the second scan are used to form a track with the two-point initialization technique.[10] The track splitting used in References 3 and 6 was found unnecessary — the strongest validated measurement was adequate. This technique yields the position and velocity estimates and the associated covariance matrices in all three coordinates.

Scan 3 (t = 0.2s) — The pointing direction for the radar is given by the predicted position at $t = 0.2\ s$ using the estimates at scan 2. An IMMPDA filter with three models discussed in the sequel is initialized with the estimates and covariance matrices obtained at the second scan. The acceleration component for the third order model is assumed zero with variance $(a_{\max})^2$, where $a_{\max} = 70\ m/s^2$ is the maximum expected acceleration of the target.

From scan 3 on, the track is maintained using the IMMPDAF as described in Section 8.4.3. In order to maintain a high SNR for the target-originated measurement during track formation, a high-energy waveform is used. Also, scan 3 dwells are used to ensure target detection. This simplified approach cannot be used if the target-originated measurement is not given at the first scan. In that case, the track formation technique in Reference 3 can be used.

Immediate revisit with sampling interval 0.1s is carried out during track formation because the initial velocity of the target is not known — in the first scan only the position is measured and there is no *a priori* velocity. This means that in the second scan the radar must be pointed at the first scan position, assuming zero velocity. Waiting longer to obtain the second measurement could result in the loss of the target-originated measurement due to incorrect pointing. Also, in order to make the IMM mode probabilities converge to the correct values as quickly as possible, the target is revisited at a high rate.

8.4.3 Track Maintenance

The true state of the target at t_k is

$$x(t_k) = \left[x(t_k)\ \ \dot{x}(t_k)\ \ \ddot{x}(t_k)\ \ y(t_k)\ \ \dot{y}(t_k)\ \ \ddot{y}(t_k)\ \ z(t_k)\ \ \dot{z}(t_k)\ \ \ddot{z}(t_k)\right]'$$

where $x(t_k)$, $y(t_k)$, and $z(t_k)$ are the positions, $\dot{x}(t_k)$, $\dot{y}(t_k)$, and $\dot{z}(t_k)$ are the velocities, and $\ddot{x}(t_k)$, $\ddot{y}(t_k)$, and $\ddot{z}(t_k)$ are the accelerations of the target in the corresponding coordinates, respectively. The measurement vector consists of the Cartesian position components at t_k and is denoted by $z(t_k)$.

Assuming that the target motion is linear in the Cartesian coordinate system, the true state of the target can be written as

$$\mathrm{x}(t_k) = F(\delta_k)\mathrm{x}(t_{k-1}) + \Gamma(\delta_k)v(t_{k-1}) \tag{8.99}$$

and the target-originated measurement is related to the state according to

$$z(t_k) = H\mathrm{x}(t_k) + w(t_k) \tag{8.100}$$

where $\delta_k = t - t_{k-1}$. The white Gaussian noise sequences $v(t_k)$ and $w(t_k)$ are independent and their covariances are $Q(\delta_k)$ and $R(t_k)$, respectively.

With the above matrices, the predicted state $\hat{\mathrm{x}}(t_k^-)$ at time t_k is

$$\hat{\mathrm{x}}(t_k^-) = F(\delta_k) + \hat{\mathrm{x}}(t_{k-1}) \tag{8.101}$$

and the predicted measurement is

$$\hat{z}(t_k^-) = H\hat{\mathrm{x}}(t_k^-) \tag{8.102}$$

with associated innovation covariance

$$S(t_k) = HP(t_k^-)H' + R(t_k) \tag{8.103}$$

where $P(t_k^-)$ is the predicted state covariance to be defined in Equation 8.117 and $R(t_k)$ is the (expected) measurement noise covariance.

8.4.3.1 Probabilistic Data Association

During track maintenance, each measurement at scan t_k is validated against the established track. This is achieved by setting up a validation region centered around the predicted measurement at t_k^-. The validation region is

$$\left[z(t_k) - \hat{z}(t_k^-)\right]' S(t_k)^{-1} \left[z(t_k) - \hat{z}(t_k^-)\right] \le \gamma \tag{8.104}$$

where $S(t_k)$ is the expected covariance of the innovation corresponding to the correct measurement and $\gamma = 16$ (0.9989 probability mass[3]) is the gate size. The appropriate covariance matrix to be used in the above is discussed in the sequel.

The set of measurements validated for the track at t_k is

$$Z(k) = \left\{z_m(t_k), m = 1,2,\ldots,m_k\right\} \tag{8.105}$$

where m_k is the number of measurements validated and associated with the track. Also, the cumulative set of validated measurements up to and including scan k is denoted by Z_1^k. All unvalidated measurements are discarded.

With these m_k validated measurements at t_k, one has the following mutually exclusive and exhaustive events:

$$\varepsilon_m(t_k) \triangleq \begin{cases} \left\{\text{measurement } z_m(t_k) \text{ is from the target}\right\} & m = 1,\ldots,m_k \\ \left\{\text{all measurements are false}\right\} & m = 0 \end{cases} \tag{8.106}$$

Using the nonparametric version of the PDAF,[4] the validated measurements are associated probabilistically to the track. The combined target state estimate is obtained as

$$\hat{x}(t_k) = \sum_{m=0}^{m_k} \beta_m(t_k)\hat{x}_m(t_k) \tag{8.107}$$

where $\beta_m(t_k)$ is the probability that the m-th validated measurement is correct and $\hat{x}_m(t_k)$ is the updated state conditioned on that event. The conditionally updated states are given by

$$\hat{x}_m(t_k) = \hat{x}(t_k^-) + W_m(t_k)v_m(t_k) \quad m = 1,2,\ldots m_k \tag{8.108}$$

where $W_m(t_k)$ is the filter gain and $v_m(t_k) = z_m(t_k) - \hat{z}_m(t_k^-)$ is the innovation associated with the m-th validated measurement. The gain, which depends on the measurement noise covariance, is

$$W_m(t_k) = P(t_k^-)H'\left[HP(t_k^-)H' + R_m(t_k)\right]^{-1} \triangleq P(t_k^-)H'S_m(t_k)^{-1} \tag{8.109}$$

where $R_m(t_k)$ depends on the observed SNR for measurement m.[8]

The association event probabilities $\beta_m(t_k)$ are given by

$$\beta_m(t_k) = P\left\{\varepsilon_m(t_k) \middle| z_1^k\right\} \tag{8.110}$$

$$= \begin{cases} \dfrac{e(m)}{b + \sum_{j=1}^{m_k} e(j)} & m = 1,2,\ldots,m_k \\ \dfrac{b}{b + \sum_{j=1}^{m_k} e(j)} & m = 0 \end{cases} \tag{8.111}$$

where

$$e(m) = N\left[\nu_m(t_k); 0, S_m(t_k)\right] \tag{8.112}$$

$$b = m_k \frac{1 - P_D}{P_D V(t_k)} \tag{8.113}$$

and P_D is the probability of detection of a target-originated measurement. The probability that a target-originated measurement, if detected, falls within the validation gate is assumed to be unity. Also, $\mathcal{N}[\nu; 0, S]$ denotes the normal pdf with argument ν, mean zero, and covariance matrix S. The common validation volume $V(t_k)$ is the union of the validation volumes $V_m(t_k)$ used to validate the individual measurements associated with the target $V(t_k)$ and is given by

$$V_m(t_k) = \gamma^{n_z/2} V_{n_z} \left|S_m(t_k)\right|^{1/2} \tag{8.114}$$

where V_{n_z} is the volume of the unit hypersphere of dimension n_z, the dimension of the measurement $\mathbf{z}$. For the three-dimensional position measurements $V_{n_z} = \frac{4\pi}{3}$ (see Reference 3).

The state estimate is updated as

$$\hat{x}(t_k) = \hat{x}(t_k^-) + \sum_{m=1}^{m_k} \beta_m(t_k) W_m(t_k) \nu_m(t_k) \tag{8.115}$$

and the associated covariance matrix is updated as

$$P(t_k) = P(t_k^-) - \sum_{m=1}^{m_k} \beta_m(t_k) W_m(t_k) S_m(t_k) W_m(t_k)' + \tilde{P}(t_k) \tag{8.116}$$

where

$$P(t_k^-) = F(\delta_k) P(t_{k-1}) F(\delta_k)' + \Gamma(\delta_k) Q(\delta_k) \Gamma(\delta_k)' \tag{8.117}$$

is the predicted state covariance and the term

$$\tilde{P}(t_k) = \sum_{m=1}^{m_k} \beta_m(t_k)\left[W_m(t_k)\nu_m(t_k)\right]\left[W_m(t_k)\nu_m(t_k)\right]' - \left[\sum_{m=1}^{m_k} \beta_m(t_k) W_m(t_k)\nu_m(t_k)\right]\left[\sum_{m=1}^{m_k} \beta_m(t_k) W_m(t_k)\nu_m(t_k)\right]' \tag{8.118}$$

is analogous to the *spread of the innovations* in the standard PDA.[3] Monopulse processing results in different accuracies (standard deviations) for different measurements within the same dwell. This accounts for the difference in the above equations from the standard PDA, where the measurement accuracies are assumed to be the same for all of the validated measurements.

To initialize the filter at $k = 3$, the following estimates are used:[10]

$$\hat{\mathbf{x}}(t_2) = \begin{bmatrix} \hat{x}(t_2) \\ \dot{\hat{x}}(t_2) \\ \ddot{\hat{x}}(t_2) \\ \hat{y}(t_2) \\ \dot{\hat{y}}(t_2) \\ \ddot{\hat{y}}(t_2) \\ \hat{z}(t_2) \\ \dot{\hat{z}}(t_2) \\ \ddot{\hat{z}}(t_2) \end{bmatrix} = \begin{bmatrix} \mathbf{z}_h^x(t_2) \\ \left(\mathbf{z}_h^x(t_2) - \mathbf{z}^x(t_1)\right)/\delta_2 \\ 0 \\ \mathbf{z}_h^y(t_2) \\ \left(\mathbf{z}_h^y(t_2) - \mathbf{z}^y(t_1)\right)/\delta_2 \\ 0 \\ \mathbf{z}_h^z(t_2) \\ \left(\mathbf{z}_h^z(t_2) - \mathbf{z}^z(t_1)\right)/\delta_2 \\ 0 \end{bmatrix} \tag{8.119}$$

where h is the index corresponding to the validated measurement with the highest SNR in the second scan, and the superscripts x, y, and z denote the components in the corresponding directions, respectively. The associated covariance matrix can be derived[10] using the measurement covariance R_h and the maximum target acceleration $a_{\max}$. If the two point differencing results in a velocity component that exceeds the corresponding maximum speed, it is replaced by that speed. Similarly, the covariance terms corresponding to the velocity components are upper bounded by the corresponding maximum values.

8.4.3.2 IMM Estimator Combined with the PDA Technique

In the IMM estimator it is assumed that at any time the target trajectory evolves according to one of a finite number of models, which differ in their noise levels and/or structures.[10] By probabilistically combining the estimates of the filters, typically Kalman, matched to these modes, an overall estimate is found. In the IMM-PDAF the Kalman filter is replaced with the PDA filter (given in Section 8.4.3.1 for mode-conditioned filtering of the states), which handles the data association.

Let r be the number of mode-matched filters used, $M(t_k)$ the index of the mode in effect in the semi-open interval (t_{k-1}, t_k) and $\mu_j(t_k)$ be the probability that mode j ($j = 1, 2, \ldots, r$) is in effect in the above interval. Thus,

$$\mu_j(t_k) = P\left\{M(t_k) = j \middle| Z_1^k\right\} \tag{8.120}$$

The mode transition probability is defined as

$$p_{ij} = P\left\{M(t_k) = j \middle| M(t_{k-1}) = i\right\} \tag{8.121}$$

The state estimates and their covariance matrix at t_k conditioned on the j-th mode are denoted by and $P_j(t_k)$, respectively.

The steps of the IMMPDAF are as follows[3]

Step 1 — Mode interaction or mixing. The mode-conditioned state estimate and the associated covariances from the previous iteration are mixed to obtain the initial condition for the mode-matched filters. The initial condition in cycle k for the PDAF matched to the j-th mode is computed using

$$\hat{\mathrm{x}}_{0j}\left(t_{k-1}\right)=\sum_{\mathrm{i}=1}^{\mathrm{r}}\hat{\mathrm{x}}_{i}\left(t_{k-1}\right)\mu_{i|j}\left(t_{k-1}\right) \tag{8.122}$$

where

$$\mu_{i|j}\left(t_{k-1}\right)=\mathrm{P}\left\{M\left(t_{k-1}\right)=i\middle|\mathrm{M}\left(t_{k-1}\right)=j,Z_1^{k-1}\right\}=\frac{p_{ij}\mu_i\left(t_{k-1}\right)}{\sum_{l=1}^{r}p_{lj}\mu_l\left(t_{k-1}\right)}\quad i,\ j=1,2,\ldots,r \tag{8.123}$$

are the mixing probabilities. The covariance matrix associated with Equation 8.122 is given by

$$P_{0j}\left(t_{k-1}\right)=\sum_{i=1}^{r}\mu_{i|j}\left(t_{k-1}\right)\left\{P_i\left(t_{k-1}\right)+\left[\hat{\mathrm{x}}_i\left(t_k\right)-\hat{\mathrm{x}}_{0j}\left(t_{k-1}\right)\right]\left[\hat{\mathrm{x}}_i\left(t_k\right)-\hat{\mathrm{x}}_{0j}\left(t_{k-1}\right)\right]'\right\} \tag{8.124}$$

Step 2 — Mode-conditioned filtering. A PDAF is used for each mode to calculate the mode-conditioned state estimates and covariances. In addition, we evaluate the likelihood function $\Lambda_j(t_k)$ of each mode at t_k using the Gaussian-uniform mixture

$$\begin{aligned}\Lambda_j\left(t_k\right)&\stackrel{\Delta}{=}p\left[Z\left(k\right)\middle|M\left(t_k\right)=j,Z_1^{k-1}\right]\\&=V\left(t_k\right)^{-m_l}\left(1-P_D\right)+V\left(t_k\right)^{1-m_k}\frac{P_D}{m_k}\sum_{m=1}^{m_k}e_j\left(m\right)\end{aligned} \tag{8.125}$$

$$=\frac{P_DV\left(t_k\right)^{1-m_k}}{m_k}\left(b+\sum_{m=1}^{m_k}e_j\left(m\right)\right) \tag{8.126}$$

where $e_j(m)$ is defined in Equation 8.112 and b in Equation 8.113. Note that the likelihood function, as a pdf, has a physical dimension that depends on m_k. Since ratios of these likelihood functions are to be calculated, they all must have the same dimension, i.e., the same m_k. Thus a common validation region (Equation 8.104) is vital for all the models in the IMMPDAF. Typically the "largest" innovation covariance matrix corresponding to "noisiest" model covers the others and, therefore, this can be used in Equations 8.104 and 8.114.

Step 3 — Mode update. The mode probabilities are updated based on the likelihood of each mode using

$$\mu_j\left(t_k\right)=\frac{\Lambda_j\left(t_k\right)\sum_{l=1}^{r}p_{lj}\mu_l\left(t_{k-1}\right)}{\sum_{l=1}^{r}\sum_{l=1}^{r}\Lambda_i\left(t_k\right)p_{lj}\mu_l\left(t_{k-1}\right)} \tag{8.127}$$

Step 4 — State combination. The mode-conditioned estimates and covariances are combined to find the overall estimate $\hat{x}(t_k)$ and its covariance matrix $P(t_k)$, as follows:

$$\hat{x}(t_k) = \sum_{j=1}^{r} \mu_j(t_k)\hat{x}(t_k) \tag{8.128}$$

$$P(t_k) = \sum_{j=1}^{r} \mu_j(t_k)\left(P_j(t_k) + \left[\hat{x}_j(t_k) - \hat{x}(t_k)\right]\left[\hat{x}_j(t_k) - \hat{x}(t_k)\right]' \right) \tag{8.129}$$

8.4.3.3 The Models in the IMM Estimator

The selection of the model structures and their parameters is one of the critical aspects of the implementation of IMMPDAF. Designing a good set of filters requires *a priori* knowledge about the target motion, usually in the form of maximum accelerations and sojourn times in various motion modes.[10] The tracks considered in the benchmark problem span a wide variety of motion modes — from benign constant velocity motions to maneuvers up to 7*g*. To handle all possible motion modes and to handle automatic track formation and termination, the following models are used:

Benign motion model (M^1) — This second-order model with low noise level (to be given later) has a probability of target detection P_D given by the target's expected SNR and corresponds to the nonmaneuvering intervals of the target trajectory. For this model the process noise is, typically, assumed to model air turbulence.

Maneuver model (M^2) — This second-order model with high noise level corresponds to ongoing maneuvers. For this white noise acceleration model, the process noise standard deviation σ_{v2} is obtained using

$$\sigma_{v2} = \alpha a_{\max} \tag{8.130}$$

where $a_{\max}$ is the maximum acceleration in the corresponding modes and $0.5 < \alpha \leq 1$.[10]

Maneuver detection model (M^3) — This is a third-order (Wiener process acceleration) model with high level noise. For highly maneuvering targets, like military attack aircraft, this model is useful for detecting the onset and termination of maneuvers. For civilian air traffic surveillance,[19] this model is not necessary.

For a Wiener process acceleration model, the standard deviation σ_{v3} is chosen using

$$\sigma_{v3} = \min\left\{\beta\Delta_a\delta, a_{\max}\right\} \tag{8.131}$$

where Δ_a is the maximum acceleration increment per unit time (jerk), δ is the sampling interval, and $0.5 < \alpha \leq 1$.[3]

For the targets under consideration, $a_{\max} = 70$ m/s^2 and $\Delta_a = 35$ m/s^3. Using these values, the process noise standard deviations were taken as

$\sigma_{v1} = 3$ m/s^2 (for nonmaneuvering intervals)

$\sigma_{v2} = 35$ m/s^2 (for maneuvering intervals)

$\sigma_{v3} = \min\{35\delta, 70\}$ (for maneuver start/termination)

In addition to the process noise levels, the elements of the Markov chain transition matrix between the modes, defined in Equation 8.121, are also design parameters. Their selection depends on the sojourn time in each motion mode. The transition probability depends on the expected sojourn time via

$$\tau_i = \frac{\delta}{1 - p_{ii}} \tag{8.132}$$

where τ_i is the expected sojourn time of the I-th mode, p_{ii} is the probability of transition from I-th mode to the same mode and δ is the sampling interval.[10]

For the above models, p_{ii}, $I = 1,2,3$ are calculated using

$$p_{ii} = \min\left\{u_{i,\max}\left(l_i, 1 - \frac{\delta}{\tau_i}\right)\right\} \tag{8.133}$$

where $l_i = 0{:}1$ and $u_i = 0{:}9$ are the lower and upper limits, respectively, for the I-th model transition probability.

The expected sojourn times of 15, 4, and 2s, are assumed for modes M^1, M^2, and M^3, respectively. The selection of the off-diagonal elements of the Markov transition matrix depends on the switching characteristics among the various modes and is done as follows:

$$p_{12} = 0.1(1 - p_{11}) \qquad p_{13} = 0.9(1 - p_{11})$$

$$p_{21} = 0.1(1 - p_{22}) \qquad p_{23} = 0.9(1 - p_{22})$$

$$p_{31} = 0.3(1 - p_{33}) \qquad p_{32} = 0.7(1 - p_{33})$$

The x, y, z components of target dynamics are uncoupled, and the same process noise is used in each coordinate.

8.4.4 Track Termination

According to the benchmark problem, a track is declared lost if the estimation error is greater than the two-way beam width in angles or 1.5 range gates in range. In addition to this problem-specific criterion, the IMMPDAF declares (on its own) track loss if the track is not updated for 100s. Alternatively, one can include a "no target" model,[3] which is useful for automatic track termination, in the IMM mode set. In a more general tracking problem, where the true target state is not known, the "no target" mode probability or the track update interval would serve as the criterion for track termination, and the IMMPDAF would provide a unified framework for track formation, maintenance, and termination.

8.4.5 Simulation Results

This section presents the simulation results obtained using the algorithms described earlier. The computational requirements and root-mean-square errors (RMSE) are given.

The tracking algorithm using the IMMPDAF is tested on the following six benchmark tracks (the tracking algorithm does not know the type of the target under track — the parameters are selected to handle any target):

Target 1 — A large military cargo aircraft with maneuvers up to 3*g*.
Target 2 — A Learjet or commercial aircraft which is smaller and more maneuverable than target 1 with maneuvers up to 4*g*.
Target 3 — A high-speed medium bomber with maneuvers up to 4*g*.
Target 4 — Another medium bomber with good maneuverability up to 6*g*.
Targets 5 and 6 — Fighter or attack aircraft with very high maneuverability up to 7*g*.

In Table 8.2, the performance measures and their averages of the IMMPDAF (in the presence of FA, RGPO, and SOJ[6,8]) are given. The averages are obtained by adding the corresponding performance metrics

TABLE 8.2 Performance of IMMPDAF in the Presence of False Alarms, Range Gate Pull-Off, and the Standoff Jammer

Target	Time Length (s)	Max. Acc. (m/s_2)	Man. Density (%)	Sample Period (s)	Avg. Power (W)	Pos. RMSE (m)	Vel. RMSE (m/s)	Ave. Load (kFLOPS)	Lost Tracks (%)
1	165	31	25	2.65	8.9	98.1	61.3	22.2	1
2	150	39	28.5	2.39	5.0	97.2	68.5	24.3	0
3	145	42	20	2.38	10.9	142.1	101.2	24.6	1
4	184	58	20	2.34	3.0	26.5	25.9	24.3	0
5	182	68	38	2.33	18.4	148.1	110.7	27.1	2
6	188	70	35	2.52	12.4	98.6	71.4	24.6	1
Avg.	—	—	—	**2.48**	**8.3**	—	—	**24.5**	—

of the six targets (with those of target 1 added twice) and dividing the sum by 7. In the table, the maneuver density is the percentage of the total time that the target acceleration exceeds $0.5g$. The average floating point operation (FLOP) count per second was obtained by dividing the total number of floating point operations by the target track length. This is the computational requirement for target and jammer tracking, neutralizing techniques for ECM, and adaptive parameter selection for the estimator, i.e., it excludes the computational load for radar emulation.

The average FLOP requirement is 25 kFLOPS, which can be compared with the FLOP rate of 78 MFLOPS of a Pentium® processor running at 133 MHz. (The FLOP count is obtained using the built-in MATLAB function flops. Note that these counts, which are given in terms of thousands of floating point operations per second (kFLOPS) or millions of floating point operations per second (MFLOPS), are rather pessimistic — the actual FLOP requirement would be considerably lower.) Thus, the real-time implementation of the complete tracking system is possible. With the average revisit interval of 2.5s, the FLOP requirement of the IMMPDAF is 62.5 kFLOP/radar cycle. With the revisit time calculations taking about the same amount of computation as a cycle of the IMMPDAF, but running at half the rate of the Kalman filter (which runs at constant rate), the IMMPDAF with adaptive revisit time is about 10 times costlier computationally than a Kalman filter. Due to its ability to save radar resources, which are much more expensive than computational resources, the IMMPDAF is a viable alternative to the Kalman filter, which is the standard "workhorse" in many current tracking systems. (Some systems still use the α-β filter as their "work mule.")

8.5 A Flexible-Window ML-PDA Estimator for Tracking Low Observable (LO) Targets

One difficulty with the ML-PDA approach of Section 8.3, which uses a set of scans of measurements as a batch, is the incorporation of noninformative scans when the target is not present in the surveillance region for some consecutive scans. For example, if the target appears within the surveillance region of the sensor after the first few scans, the estimator can be misled by the pure clutter in those scans — the earlier scans contain no relevant information, and the incorporation of these into the estimator not only increases the amount of processing (without adding any more information), but also results in less accurate estimates or even track rejection. Also, a target could disappear from the surveillance region for a while during tracking and reappear sometime later. Again, these intervening scans contain little or no information about the target and can potentially mislead the tracker.

In addition, the standard ML-PDA estimator assumes that the target SNR, the target velocity, and the density of false alarms over the entire tracking period remain constant. In practice, this may not be the case, and then the standard ML-PDA estimator will not yield the desired results. For example, the average target SNR may vary significantly as the target gets closer to or moves away from the sensor. In addition, the target might change its course and/or speed intermittently over time. For electro-optical sensors, depending on the time of the day and weather, the number of false alarms may vary as well.

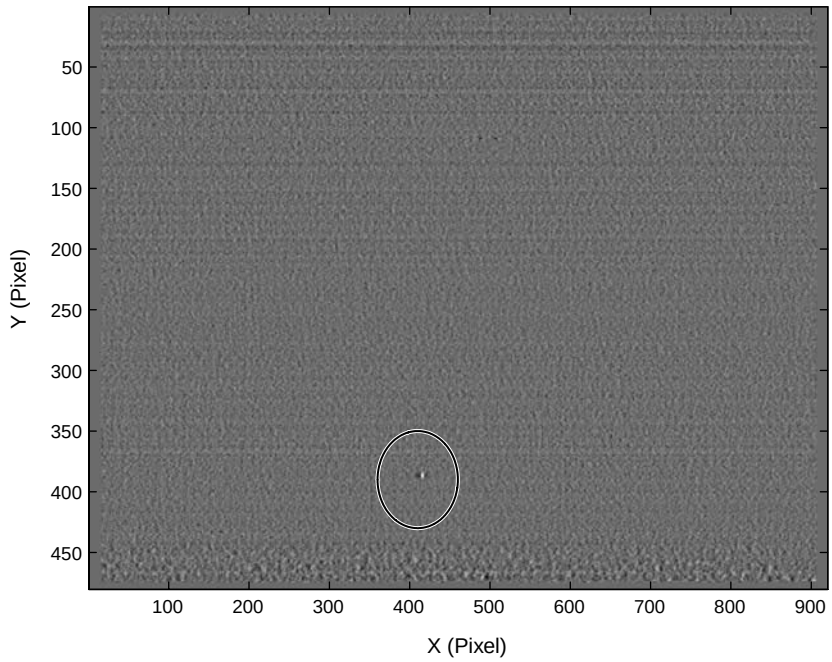

FIGURE 8.2 The last frame in the F1 Mirage sequence.

Because of these concerns, an estimator capable of handling time-varying SNR (with online adaptation), false alarm density, and slowly evolving course and speed is needed. While a recursive estimator like the IMM-PDA is a candidate, in order to operate under low SNR conditions in heavy clutter, a batch estimator is still preferred. In this section, the above problems are addressed by introducing an estimator that uses the ML-PDA with AI *adaptively* in a sliding-window fashion,[20] rather than using all the measurements in a single batch as the standard ML-PDA estimator does.[14] The initial time and the length of this sliding window are adjusted adaptively based on the information content in the measurements in the window. Thus, scans with little or no information content are eliminated and the window is moved over to scans with "informative" measurements.

This algorithm is also effective when the target is temporarily lost and reappears later. In contrast, recursive algorithms will diverge in this situation and may require an expensive track reinitiation. The standard batch estimator will be oblivious to the disappearance and may lose the whole track. This section demonstrates the performance of the adaptive sliding-window ML-PDA estimator on a real scenario with heavy clutter for tracking a fast-moving aircraft using an electro-optical (EO) sensor.

8.5.1 The Scenario

The adaptive ML-PDA algorithm was tested on an actual scenario consisting of 78 frames of Long Wave Infrared (LWIR) IR data collected during the Laptex data collection, which occurred in July, 1996 at Crete, Greece. The sequence contains a single target — a fast-moving Mirage F1 fighter jet. The 920 × 480 pixel frames, taken at a rate of 1Hz were registered to compensate for frame-to-frame line-of-sight (LOS) jitter. Figure 8.2 shows the last frame in the F1 Mirage sequence.

A sample detection list for the Mirage F1 sequence obtained at the end of preprocessing is shown in Figure 8.3. Each "x" in the figure represents a detection above the threshold.

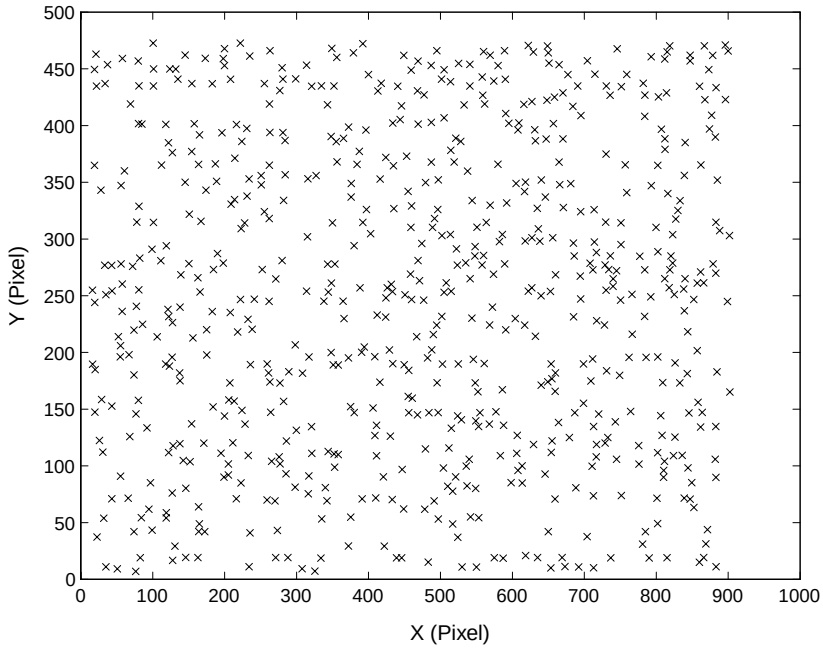

FIGURE 8.3 Detection list corresponding to the frame in Figure 8.2.

8.5.2 Formulation of the ML-PDA Estimator

This section describes the target models used by the estimator in the tracking algorithm and the statistical assumptions made by the algorithm. The ML-PDA estimator for these models is introduced, and the CRLB for the estimator and the hypothesis test used to validate the track are presented.

8.5.2.1 Target Models

The ML-PDA tracking algorithm is used on the detection lists after the data preprocessing phase. It is assumed that there are n detection lists obtained at times $t = t_1,t_2,\ldots t_n$. The i-th detection list, where $1 \le i \le n$, consists of m_i detections at pixel positions (x_{ij}, y_{ij}) along the X and Y directions. In addition to locations, the signal strength or amplitude, a_{ij}, of the j-th detection in the i-th list, where $1 \le j \le m$, is also known. Thus, assuming constant velocity over a number of scans, the problem can be formulated as a two-dimensional scenario in space with the target motion defined by the four-dimensional vector

$$\mathbf{x} \triangleq \left[\xi(t_0)\eta(t_0)\dot{\xi}\dot{\eta}\right]' \tag{8.134}$$

where $\xi(t_0)$ and $\eta(t_0)$ are the horizontal and vertical pixel positions of the target, respectively, from the origin at the reference time t_0. The corresponding velocities along these directions are assumed constant at $\dot{\xi}(t_o)$ pixel/s and $\dot{\eta}(t_o)$ pixel/s, respectively.

The set of measurements in list i at time t_i is denoted by

$$Z(i) = \left\{z_j(i)\right\}_{j=1}^{m_i} \tag{8.135}$$

where m_i is the number of measurements at t_i. The measurement vector $z_j(i)$ is denoted by

$$z_j(i) \triangleq \begin{bmatrix} x_{ij} & y_{ij} & a_{ij} \end{bmatrix}' \tag{8.136}$$

where x_{ij} and y_{ij} are observed X and Y positions, respectively.

The cumulative set of measurements made in scans t_1 through t_{-n} is given by

$$Z^n = \left\{ Z(i) \right\}_{i=1}^{n} \tag{8.137}$$

A measurement can either originate from a true target or from a spurious source. In the former case, each measurement is assumed to have been received only once in each scan with a detection probability P_D and to have been corrupted by zero-mean additive Gaussian noise of known variance, i.e.,

$$x_{ij} = \xi(t_i) + \in_{ij} \tag{8.138}$$

$$y_{ij} = \eta(t_i) + v_{ij} \tag{8.139}$$

where $\in_{ij}$ and v_{ij} are the zero-mean Gaussian noise components with variances σ_1^2 and σ_2^2 along the X and Y directions, respectively.

Thus, the joint probability density function of the position components of z_{ij} is given by

$$p(z_{ij}) = \frac{1}{2\pi\sigma_1\sigma_2} \exp\left(-\frac{1}{2}\left[\frac{x_{ij} - \xi(t_i)}{\sigma_1} \right]^2 - \frac{1}{2}\left[\frac{y_{ij} - \eta(t_i)}{\sigma_2} \right]^2 \right) \tag{8.140}$$

The false alarms are assumed to be distributed uniformly in the surveillance region and their number at any sampling instant obeys the Poisson probability mass function

$$\mu_f(m_i) = \frac{(\lambda U)^{m_i} e^{-\lambda U}}{m_i!} \tag{8.141}$$

where U is the area of surveillance and λ is the expected number of false alarms per unit of this area. Kirubarajan and Bar-Shalom[14] have shown that the performance of the ML-PDA estimator can be improved by using amplitude information (AI) of the received signal in the estimation process itself, in addition to thresholding. After the signal has been passed through the matched filter, an envelope detector can be used to obtain the amplitude of the signal. The noise at the matched filter is assumed to be narrowband Gaussian. When this is fed through the envelope detector, the output is Rayleigh distributed. Given the detection threshold, τ, the probability of detection P_D and the probability of false alarm P_{FA} are

$$P_D \triangleq P(\text{The target-oriented measurement exceeds the threshold } \tau) \tag{8.142}$$

and

$$P_{FA} \triangleq P(\text{A measurement caused by noise only exceeds the threshold } \tau) \tag{8.143}$$

where $P(\cdot)$ is the probability of an event.

The probability density functions at the output of the threshold detector, which corresponds to signals from the target and false alarms are denoted by $p_1^{\tau}(a)$ and $p_0^{\tau}(a)$, respectively. Then the amplitude likelihood ratio, ρ, can then be written as[3]

$$\rho = \frac{p_1^{\tau}(a)}{p_0^{\tau}(a)} = \frac{P_{FA}}{P_D(1+d)} \exp\left(\frac{a^2 d}{2(1+d)}\right) \tag{8.144}$$

where τ is the detection threshold.

8.5.2.2 The Maximum Likelihood-Probabilistic Data Association Estimator

This section focuses on the maximum likelihood estimator combined with the PDA approach. If there are m_i detections at t_i, one has the following mutually exclusive and exhaustive events[3]

$$\varepsilon_j(i) \triangleq \begin{cases} \{\text{measurement } z_j(i) \text{ is from the target}\} & j = 1,\ldots,m_i \\ \{\text{all measurements are false}\} & j = 0 \end{cases} \tag{8.145}$$

The pdf of the measurements corresponding to the above events can be written as[3]

$$p\left(Z(i)\middle|\varepsilon_j(i),\mathbf{x}\right) = \begin{cases} U^{1-m_i} p(z_{ij}) \rho_{ij} \prod_{j=1}^{m_i} p_0^{\tau}(a_{ij}) & j = 1,\ldots,m_i \\ U^{1-m_i} \prod_{j=1}^{m_i} p_0^{\tau}(a_{ij}) & j = 0 \end{cases} \tag{8.146}$$

Using the total probability theorem,

$$\begin{aligned} p(Z(i)|\mathbf{x}) &= \sum_{j=0}^{m_i} p\left(Z(i)\middle|\varepsilon_j(i),\mathbf{x}\right) p\left(\varepsilon_j(i),\mathbf{x}\right) \\ &= \sum_{j=0}^{m_i} p\left(Z(i)\middle|\varepsilon_j(i),\mathbf{x}\right) p\left(\varepsilon_j(i)\right) \end{aligned} \tag{8.147}$$

the above can be written explicitly as

$$\begin{aligned} p(Z(i)|\mathbf{x}) &= U^{-mi}(1-P_D) \prod_{j=1}^{m_i} p_0^{\tau}(a_{ij}) \mu_f(m_i) + \frac{U^{1-m_i} P_D \mu_f(m_i - 1)}{m_i} \prod_{j=1}^{m_i} p_0^{\tau}(a_{ij}) \sum_{j=1}^{m_i} p(z_{ij}) \rho_{ij} \\ &= U^{-mi}(1-P_D) \prod_{j=1}^{m_i} p_0^{\tau}(a_{ij}) \mu_f(m_i) + \frac{U^{1-m_i} P_D \mu_f(m_i - 1)}{2\pi\sigma_1\sigma_2 m_i} \prod_{j=1}^{m_i} p_0^{\tau}(a_{ij}) \\ &\quad \cdot \sum_{j=1}^{m_i} \rho_{ij} \exp\left(-\frac{1}{2}\left[\frac{x_{ij} - \xi(t_i)}{\sigma_1}\right]^2 - \frac{1}{2}\left[\frac{y_{ij} - \eta(t_i)}{\sigma_2}\right]^2\right) \end{aligned} \tag{8.148}$$

To obtain the likelihood ratio, $\Phi[Z(i), \mathbf{x}]$, at t_i, divide Equation 8.148 by $p[Z(i)|\varepsilon_0(i), \mathbf{x}]$

$$\begin{aligned}\Phi\left[Z(i),\mathbf{x}\right] &= \frac{p\left[Z(i),\mathbf{x}\right]}{p\left[Z(i)\middle|\varepsilon_0(i),\mathbf{x}\right]} \\ &= \left(1-P_D\right)+\frac{P_D}{2\pi\lambda\sigma_1\sigma_2}\sum\rho_{ij}\exp\left(-\frac{1}{2}\left[\frac{x_{ij}-\xi(t_i)}{\sigma_1}\right]^2-\frac{1}{2}\left[\frac{y_{ij}-\eta(t_i)}{\sigma_2}\right]^2\right)\end{aligned} \tag{8.149}$$

Assuming that measurements at different sampling instants are conditionally independent, i.e.,

$$p\left[Z^n\middle|\mathbf{x}\right]=\prod p\left[Z(i)\middle|\mathbf{x}\right] \tag{8.150}$$

the total likelihood ratio[3] for the entire data set is given by

$$\Phi\left[Z^n,\mathbf{x}\right]=\prod_{i=1}^{n}\Phi_i\left[Z(i),\mathbf{x}\right] \tag{8.151}$$

Then, the total log-likelihood ratio, $\Phi[Z^n, \mathbf{x}]$, expressed in terms of the individual log-likelihood ratios $\phi[Z(i), \mathbf{x}]$ at sampling time instants t_i, becomes

$$\begin{aligned}\phi\left[Z^n,\mathbf{x}\right] &= \sum_{i=1}^{n}\phi_i\left[Z(i),\mathbf{x}\right] \\ &= \sum\ln\left[\left(1-P_D\right)+\frac{P_D}{2\pi\lambda\sigma_1\sigma_2}\sum_{j=1}^{m_i}\rho_{ij}\exp\left(-\frac{1}{2}\left[\frac{x_{ij}-\xi(t_i)}{\sigma_1}\right]^2-\frac{1}{2}\left[\frac{y_{ij}-\eta(t_i)}{\sigma_2}\right]^2\right)\right]\end{aligned} \tag{8.152}$$

The maximum likelihood estimate (MLE) is obtained by finding the vector $\mathbf{x} = \hat{\mathbf{x}}$ that maximizes the total log-likelihood ratio given in Equation 8.152. This maximization is performed using a quasi-Newton (variable metric) method. This can also be accomplished by minimizing the negative log-likelihood function. In our implementation of the MLE, the Davidon-Fletcher-Powell variant of the variable metric method is used. This method is a conjugate gradient technique that finds the minimum value of the function iteratively.[21] However, the negative log-likelihood function may have several local minima; i.e., it has multiple modes. Due to this property, if the search is initiated too far away from the global minimum, the line search algorithm may converge to a local minimum. To remedy this, a multi-pass approach is used as in Reference 14.

8.5.3 Adaptive ML-PDA

Often, the measurement process begins before the target becomes visible — that is, the target enters the surveillance region of the sensor some time after the sensor started to record measurements. In addition, the target may disappear from the surveillance region for a certain period of time before reappearing.

During these periods of blackout, the received measurements are purely noise-only, and the scans of data contain no information about the target under track. Incorporating these scans into a tracker reduces its accuracy and efficiency. Thus, detecting and rejecting these scans is important to ensure the fidelity of the estimator. This subsection presents a method that uses the ML-PDA algorithm in a sliding-window fashion. In this case, the algorithm uses only a subset of the data at a time rather than all of the frames at once, to eliminate the use of scans that have no target. The initial time and the length of the sliding window are adjusted adaptively based on the information content of the data — the smallest window, and thus the fewest number of scans, required to identify the target is determined online and adapted over time.

The key steps in the adaptive ML-PDA estimator are as follows:

1. Start with a window of minimum size.
2. Run the ML-PDA estimator within this window and carry out the validation test on the estimates.
3. If the estimate is accepted (i.e., if the test is passed), and if the window is of minimum size, accept the window. The next window is the present window advanced by one scan. Go to step 2.
4. If the estimate is accepted, and if the window is greater than minimum size, try a shorter window by removing the initial scan. Go to step 2 and accept the window only if estimates are better than those from the previous window.
5. If the test fails and if the window is of minimum size, increase the window length to include one more scan of measurements and, thus, increase the information content in the window. Go to step 2.
6. If the test fails and if the window is greater than minimum size, eliminate the first scan, which could contain pure noise only. Go to step 2.
7. Stop when all scans are used.

The algorithm is described below. In order to specify the exact steps in the estimator, the following variables are defined:

W = Current window length
$W_{\min}$ = Minimum window length
$Z(t_i)$ = Scan (set) of measurements at time t_i

With these definitions, the algorithm is given below:

BEGIN PROCEDURE Adaptive ML PDA estimator($W_{\min}$, $Z(t_1)$, $Z(t_n)$)
  $i = 1$ — Initialize the window at the first scan.
  $W = W_{\min}$ — Initially, use a window of minimum size.
  WHILE ($i + W < n$) — Repeat until the last scan at t_n.
    Do grid search for initial estimates by numerical search on $Z(t_i)$, $Z(t_{i+1}),\ldots,Z(t_{i+W})$
    Apply ML-PDA Estimator on the measurements in $Z(t_i)$, $Z(t_{i+1}),\ldots,Z(t_{i+W})$
    Validate the estimates
    IF the estimates are rejected
      IF ($W > W_{\min}$) — Check if we can reduce the window size.
        $i = i + 1$ — Eliminate the initial scan that might be due to noise only.
      ELSEIF ($W = W_{\min}$)
        $W = W + 1$ — Expand window size to include an additional scan.
      ENDIF
    ENDIF
    IF the estimates are accepted
      IF ($W > W_{\min}$) — Check if we can reduce the window size.
        Try a shorter window by removing the initial scan and check if estimates are better, $i = i + 1$
      ENDIF

```
            IF estimates for shorter window are NOT better OR (W = W_min)
                Accept estimates and try next window, i = i + 1
            ENDIF
        ENDIF
    END WHILE
END PROCEDURE
```

To illustrate the adaptive algorithm, consider a scenario where a sensor records 10 scans of measurements over a surveillance region. The target, however, appears in this region (i.e., its intensity exceeds the threshold) only after the second scan (i.e., from the third scan onward). This case is illustrated in Figure 8.4. The first two scans are useless because they contain only noise.

Consider the smallest window size required for a detection to be 5. Then the algorithm will evolve as shown in Figure 8.5. First, for the sake of illustration, assume that a single "noisy" scan present in the data set is sufficient to cause the MLE to fail the hypothesis test for track acceptance. The algorithm tries to expand the window to include an additional scan if a track detection is not made. This is done because an additional scan of data may bring enough additional information to detect the target track. The algorithm next tries to cut down the window size by removing the initial scans. This is done to check whether a better estimate can be obtained without this scan. If this initial scan is noise only, then it degrades the accuracy of the estimate. If a better estimate is found (i.e., a more accurate estimate) without this scan, the latter is eliminated. Thus, as in the example given above, the algorithm expands at the front (most recent scan used) and contracts at the rear end of the window to find the best window that produces the strongest detection, based on the validation test.

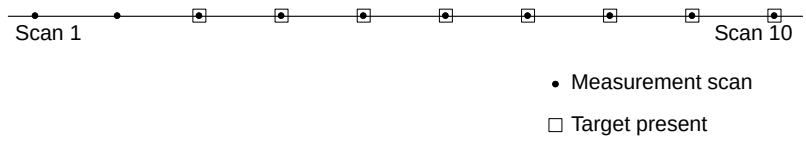

FIGURE 8.4 Scenario with a target being present for only a partial time during observation.

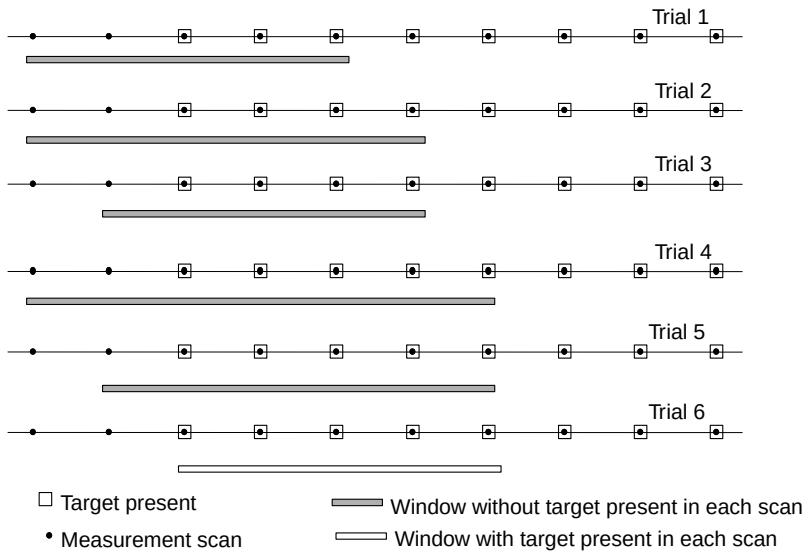

FIGURE 8.5 Adaptive ML-PDA algorithm applied to the scenario illustrated above.

TABLE 8.3 Parameters Used in the ML-PDA Algorithm for the F1 Mirage Jet

Parameter	Value
σ_1	1.25
σ_2	1.25
Min Window Size, W	10
Initial Target SNR, d_0	9.5
P_{DC}	0.70
α	0.85
π_m	5%
$\bar{\nu}$	5.0
$\bar{\sigma}_\nu$	0.15
K	4

8.5.4 Results

8.5.4.1 Estimation Results

The Mirage F1 data set consists of 78 scans or frames of LWIR IR data. The target appears late in this scenario and moves towards the sensor. There are about 600 detections per frame. In this implementation the parameters shown in Table 8.3 were chosen.

The choice of these parameters is explained below:

- σ_1 and σ_2 are, as in Equation 8.140, the standard deviations along the horizontal and vertical axes respectively. The value of 1:25 for both variables models the results of the preprocessing.
- The minimum window size, W_{min}, was chosen to be 10. The algorithm will expand this window if a target is not detected in 10 frames. Initially a shorter window was used, but the estimates appeared to be unstable. Therefore, fewer than 10 scans is assumed to be ineffective at producing an accurate estimate.
- The initial target SNR, d_0, was chosen as 9:5 dB because the average SNR of all the detections over the frames is approximately 9:0 dB. However, in most frames, random spikes were noted. In the first frame, where a target is unlikely to be present, a single spike of 15:0 dB is noted. These spikes, however, cannot and should not be modeled as the target SNR.
- A constant probability of detection (P_{DC}) of 0:7 was chosen. A value that is too high would bring down the detection threshold and increase P_{FA}.
- α is the parameter used to update the estimated target SNR with an α filter. A high value is chosen for the purpose of detecting a distant target that approaches the sensor over time and to account for the presence of occasional spikes of noise. Thus, the estimated SNR is less dependent on a detection that could originate from a noisy source and, thus, set the bar too high for future detections.
- π_m is the miss probability.
- $\bar{\nu}$ and $\bar{\sigma}_\nu$ are used in the multipass approach of the optimization algorithm.[11,14]
- The number of passes K in the multipass approach of the optimization algorithm was chosen as 4.

Figure 8.6 further clarifies the detection process by depicting the windows where the target has been detected.

From the above results, note the following:

- The first detection uses 22 scans and occurs at scan 28. This occurs because the initial scans have low-information content as the target appears late in the frame of surveillance. The IMM-MHT algorithm[22] required 38 scans for a detection, while the IMMPDA[23] required 39 scans. Some spurious detections were noticed at earlier scans, but these were rejected.

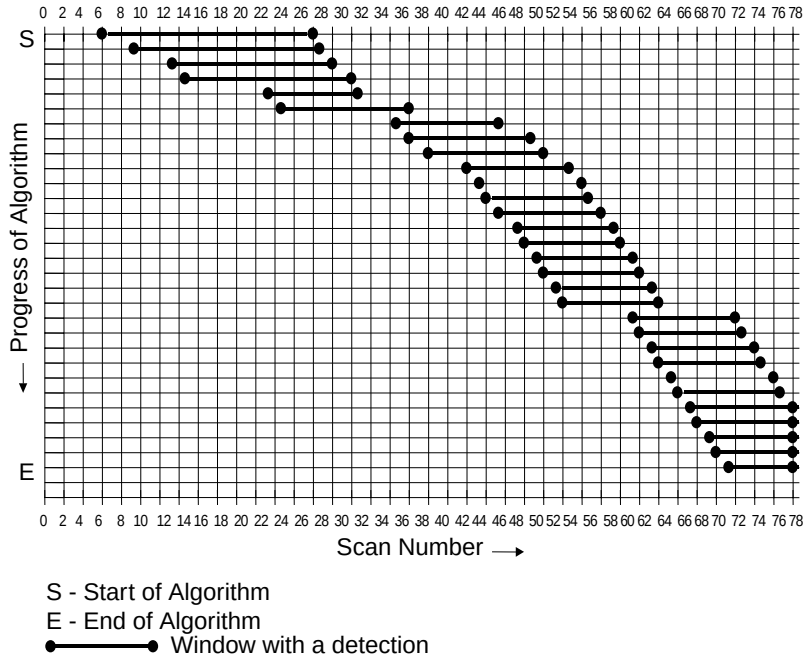

FIGURE 8.6 Progress of the algorithm showing windows with detections.

- The next few detection windows produce similar target estimates. This is because a large number of scans repeat themselves in these windows.
- After the initial detections, there is a "jump" in the scan number at which a detection is made. In addition, the estimates, particularly the velocity estimates, deteriorate. This could indicate either that the target has suddenly disappeared (became less visible) from the region of surveillance or that the target made a maneuver.
- From scan 44 onward, the algorithm stabilizes for several next windows. At scan 52, however, there is another jump in detection windows. This is also followed by a drop in the estimated target SNR, as explained above. This, however, indicates that the algorithm can adjust itself and restart after a target has become suddenly invisible. Recursive algorithms will diverge in this case.
- From scan 54 onward, the algorithm stabilizes, as indicated by the estimates. Also, a detection is made for every increasing window because the target has come closer to the sensor and, thus, is more visible. This is noted by the sharp rise in the estimated target SNR after scan 54.
- The above results provide an understanding of the target's behavior. The results suggest that the Mirage F1 fighter jet appears late in the area of surveillance and moves towards the sensor. However, initially it remains quite invisible and possibly undergoes maneuvers. As it approaches the sensor, it becomes more and more visible and, thus, easier to detect.

8.5.4.2 Computational Load

The adaptive ML-PDA tracker took 442s, including the time for data input/output, on a Pentium® III processor running at 550MHz to process the 78 scans of the Mirage F1 data. This translates into about 5.67s per frame (or 5.67s running time for one-second data), including input/output time. A more efficient implementation on a dedicated processor can easily make the algorithm real-time capable on a similar processor. Also, by parallelizing the initial grid search, which required more than 90% of the time, the adaptive ML-PDA estimator can be made even more efficient.

8.6 Summary

This chapter presented the use of the PDA technique for different tracking problems. Specifically, the PDA approach was used for parameter estimation as well as recursive state estimation. As an example of parameter estimation, track formation of a low observable target using a nonlinear maximum likelihood estimator in conjunction with the PDA technique with passive (sonar) measurements was presented. The use of the PDA technique in conjunction with the IMM estimator, resulting in the IMMPDAF, was presented as an example of recursive estimation on a radar-tracking problem in the presence of ECM. Also presented was an adaptive sliding-window PDA-based estimator that retains the advantages of the batch (parameter) estimator while being capable of tracking the motion of maneuvering targets. This was illustrated on an EO surveillance problem. These applications demonstrate the usefulness of the PDA approach for a wide variety of real tracking problems.

References

1. Bar-Shalom, Y. (Ed.), *Multitarget-Multisensor Tracking: Advanced Application*s, Vol. I, Artech House Inc., Dedham, MA, 1990. Reprinted by YBS Publishing, 1998.
2. Bar-Shalom, Y. (Ed.), *Multitarget-Multisensor Tracking: Applications and Advance*s, Vol. II, Artech House Inc., Dedham, MA, 1992. Reprinted by YBS Publishing, 1998.
3. Bar-Shalom, Y. and Li, X. R., *Multitarget-Multisensor Tracking: Principles and Techniqu*es, Storrs, CT: YBS Publishing, 1995.
4. Blackman, S. S. and Popoli, R., *Design and Analysis of Modern Tracking System*s, Artech House Inc., Dedham, MA, 1999.
5. Feo, M., Graziano, A., Miglioli, R., and Farina, A., IMMJPDA vs. MHT and Kalman Filter with NN Correlation: Performance Comparison, *IEE Proc. on Radar, Sonar and Navigation (Part F)*, 144(2), 49–56, 1997.
6. Kirubarajan, T., Bar-Shalom, Y., Blair, W. D., and Watson, G. A., IMMPDA Solution to Benchmark for Radar Resource Allocation and Tracking in the Presence of ECM, *IEEE Trans. Aerospace and Electronic System*s, 34(3), 1023–1036, 1998.
7. Lerro, D., and Bar-Shalom, Y., Interacting Multiple Model Tracking with Target Amplitude Feature, *IEEE Trans. Aerospace and Electronic System*s, AES-29, No. 2, 494–509, 1993.
8. Blair, W. D., Watson, G. A., Kirubarajan, T., and Bar-Shalom, Y., Benchmark for radar resource allocation and tracking in the presence of ECM, *IEEE Trans. Aerospace and Electronic System*s, 34(3), 1015–1022, 1998.
9. Blackman, S. S., Dempster, R. J., Busch, M. T., and Popoli, R. F., IMM/MHT solution to radar benchmark tracking problem, *IEEE Trans. Aerospace and Electronic System*s, Vol. 35(2), 730–738, 1999.
10. Bar-Shalom, Y. and Li, X. R., *Estimation and Tracking: Principles, Techniques and Softwar*e, Artech House, Dedham, MA, 1993. Reprinted by YBS Publishing, 1998.
11. Jauffret, C., and Bar-Shalom, Y., Track formation with bearing and frequency measurements in clutter, *IEEE Trans. Aerospace and Electronic Systems,* AES-26, 999–1010, 1990.
12. Kirubarajan, T., Wang, Y., and Bar-Shalom, Y., Passive ranging of a low observable ballistic missile in a gravitational field using a single sensor, *Proc. 2nd International Conf. Information Fusio*n, July 1999.
13. Sivananthan, S., Kirubarajan, T., and Bar-Shalom, Y., A radar power multiplier algorithm for acquisition of LO ballistic missiles using an ESA radar, *Proc. IEEE Aerospace Conf.*, March 1999.
14. Kirubarajan, T., and Bar-Shalom, Y., Target motion analysis in clutter for passive sonar using amplitude information, *IEEE Trans. Aerospace and Electronic System*s, 32(4), 1367–1384, 1996.
15. Nielsen, R. O., *Sonar Signal Processing*, Artech House Inc., Boston, MA, 1991.
16. Blair, W. D., Watson, G. A., and Hoffman, S. A., Benchmark problem for beam pointing control of phased array radar against maneuvering targets, *Proc. Am. Control Conf.*, June 1994.

17. Blair, W. D., and Watson, G. A., IMM algorithm for solution to benchmark problem for tracking maneuvering targets, *Proc. SPIE Acquisition, Tracking and Pointing Conf.*, April, 1994.
18. Blair, W. D., Watson, G. A., Hoffman, S. A., and Gentry, G. L., Benchmark problem for beam pointing control of phased array radar against maneuvering targets in the presence of ECM and false alarms, *Proc. American Control Conf.*, June 1995.
19. Yeddanapudi, M., Bar-Shalom, Y., and Pattipati, K. R., IMM estimation for multitarget-multisensor air traffic surveillance, *Proc. IEE*E, 85(1), 80–94, 1997.
20. Chummun, M. R., Kirubarajan, T., and Bar-Shalom, Y., An adaptive early-detection ML-PDA estimator for LO targets with EO sensors, *Proc. SPIE Conf. Signal and Data Processing of Small Target*s, April 2000.
21. Press, W. H., Teukolsky, S. A., Vetterling, W. T., and, Flannery, B. P., *Numerical Recipes in* C, Cambridge University Press, Cambridge, U.K., 1992.
22. Roszkowski, S. H., Common database for tracker comparison, *Proc. SPIE Conf. Signal and Data Processing of Small Target*s, Vol. 3373, April 1998.
23. Lerro, D., and Bar-Shalom, Y., IR Target detection and clutter reduction using the interacting multiple model estimator, *Proc. SPIE Conf. on Signal and Data Processing of Small Target*s, Vol. 3373, April 1998.